2016

Synthesis of high surface area nanomaterials and their application in catalysis

Umesh Chaudhary
Iowa State University

Synthesis of high surface area nanomaterials and their application in catalysis

by

Umesh Chaudhary

A thesis submitted to the graduate faculty

in partial fulfillment of the requirements for the degree of

MASTER OF SCIENCE

Major: Chemistry

Program of Study Committee:
Igor Slowing, Co-Major Professor
Aaron Sadow, Co-Major Professor
Young-Jin Lee

Iowa State University

Ames, Iowa

2016

DEDICATION

To my Father (Ram Narayan Chaudhary)

and Mother (Phul Kumari Chaudhary)

TABLE OF CONTENTS

ACKNOWLEDGMENTS

I would like to express my deepest gratitude to my advisor, Dr. Igor Slowing. I thank him for introducing me to the wonders and frustrations of scientific research. I thank him for his continuous patience, guidance and support throughout the course of this research and graduate career.

I would like to thank my committee members Dr. Aaron Sadow and Dr. Young Jin Lee for their valuable time and suggestions. I would also like to thank Dr. Kapil Kandel for his guidance when I was a new comer in Dr. Slowing's group and Dr. Naftali Opembe for being always available for healthy discussions about research and life as well.

I would like to thank again Dr. Aaron Sadow for letting me use their FT-IR instrument and other equipments in his lab whenever needed. I would like to thank Dr. James Anderegg for XPS analysis, Dr. Matt Besser for training and letting me use XRD instruments, Nicholas C. Nelson for TEM studies. I would like to thank my colleagues, the department faculty and staff for making my time at Iowa State University a wonderful experience. Thanks to Joseph Shrestha for helping me in formatting this document.

Thanks to U.S. Department of Energy, Ames Laboratory (Contract No. DE-AC02-07CH11358) for the funding of the projects in this dissertation.

Many thanks to my Father, Mother, and Sister (Ranjita Chaudhary) for their encouragement and unconditional love.

Finally, I would like to thank my partner in crime (Isha Shrestha). She was always there cheering me up and stood by me through good and bad times.

CHAPTER 1
GENERAL INTRODUCTION

Dissertation Organization

The dissertation is organized in 4 chapters. Chapter 1 highlights the motivations behind our research along with a general introduction on ceria and carbon catalysts. Chapter 2 reports the investigations on Copper-Ceria catalysts for the selective hydrogenation of fatty acids into fatty alcohols. Chapter 3 discusses the development of nitrogen containing mesoporous carbon. The chapter also reports the catalytic investigations for aldol condensation and nitrobenzene hydrogenation reactions. Finally, Chapter 4 is a general conclusion summarizing this dissertation.

Introduction

Catalysis plays an important role in chemical industry. Currently, about 90 % of chemical manufacturing process and 20 % of all industrial products involve catalytic steps.[1] Numerous catalysts are in constant development to fulfill economic and environmental demands. Catalysts can be categorized into two groups: Homogeneous and Heterogeneous catalysts. If the catalyst is in the same phase as the reactants then it is called homogeneous catalyst whereas if the catalyst is in a different phase than the reactants it is called heterogeneous. Homogeneous catalysis has been thoroughly studied, and its understanding created a new era in organic synthesis. Despite the impressive accomplishments, these sophisticated homogeneous systems have some limitations. Costs associated with separation, regeneration and large waste management have been long standing issues in such systems. In contrast, solid heterogeneous catalysts can be easily separated from reaction media and

repeatedly re-used, thus decreasing chemical waste and most importantly, the overall cost. These simple properties have attracted researchers to develop heterogeneous catalysts for various applications.

Nanomaterials are widely applied as heterogeneous catalysts. Because of their size these materials have high surface areas in comparison to similar masses of bulk materials. The increase in surface area per mass of a material helps in bringing the more active components from the material in contact with the reaction surroundings, thus affecting the reactivity.[1] Ceria and carbon based catalysts are among the numerous heterogeneous catalysts that have been thoroughly investigated. This chapter will highlight their potential catalytic applications.

Cerium dioxide as a support for fatty alcohol production

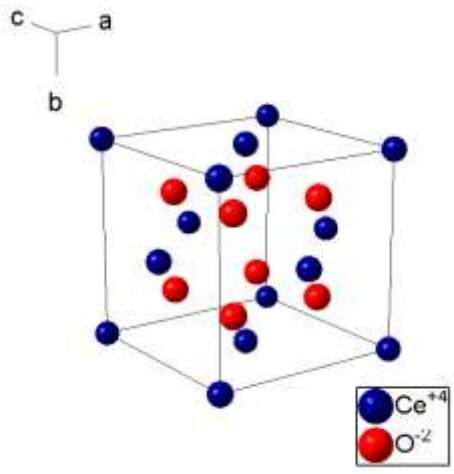

Figure 1 Crystal structure of ceria[2]

Cerium dioxide (Ceria, CeO_2) is the most abundant element in the rare earth family. Its abundance on the earth's crust is 66.5 ppm.[3] Ceria has a fluorite type crystal structure with a space group of *Fm3m* with the lattice parameter of 5.411 Å.[2] In the Figure 1, cerium

ions (Ce^{4+}) occupy the vertices and faces of cubic unit cell. Each of them is coordinated with eight oxygen ions arranged in a cube, while each oxygen ion is surrounded by four cerium ions in tetrahedral arrangement.

Ceria is an interesting material for heterogeneous catalysis. It is primarily known for its use in three way emission control, water gas shift, hydrocarbon reforming and oxidation catalysts.[4] Ceria materials possess a high oxygen storage capacity (OSC).[2] The OSC is a measure of how much oxygen a material can store and release. Due to this property, ceria can mediate reductions through the uptake of oxygen and oxidations through the release of oxygen.

Metals/metal oxides supported on ceria are of particular interest as ceria not only acts as a support for dispersion but also may take part in reactions.[5] For example, Copper oxide supported on ceria is one of the most studied ceria based catalysts due to its properties like oxygen diffusibility and reducibility.[6,7] Despite of the hydrogenation activities shown by ceria based catalysts,[8] copper ceria catalysts have been only notably used for oxidation reactions only.[9,10] Chapter 2 will provide the report on the investigations on hydrogenation reaction of fatty acids into the corresponding fatty alcohols.

Motivation: Fatty Alcohol Production

Fatty alcohols have carbon chains between 6 and 22 atoms and are typically derived from biological matter (Figure 2).

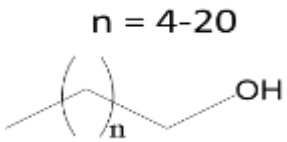

Figure 2 Generic structure of fatty alcohol

These alcohols are industrially very important as intermediates in important chemical synthesis like surfactants, detergents, fuel additives, thickeners and cosmetics.[11] The current global market value of fatty alcohols is around 1.9 billion dollars with projected growth rate of 7.3 % per year.[12]

Catalytic hydrogenation is a well-developed process for fatty alcohol production.[13] Lipid based feedstocks which are mostly composed of free fatty acids (FFAs) and triglycerides are considered major sources for fatty alcohols.[11] First, triglycerides and fatty acids are reacted with methanol to produce fatty acid methyl esters (FAMES) which are later subjected to catalytic hydrogenation to ultimately produce alcohols as shown in Figure 3. Hydrogenation of the fatty acids or esters into alkanes have been intensively studied by many research groups.[14] They have reported alcohols as intermediate products that get reduced into alkanes during hydrogenation process. In this context, we want to develop catalysts that can reduce fatty acids under molecular hydrogen where the reaction product is expected to stop at the alcohol stage.

Step 1: Transesterification

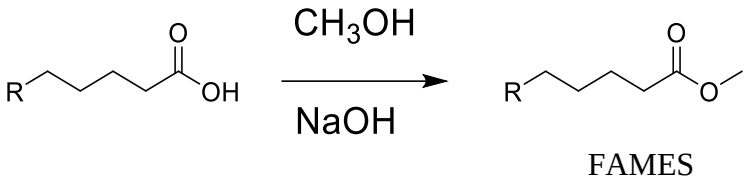

FAMES

Step 2: Catalytic hydrogenation

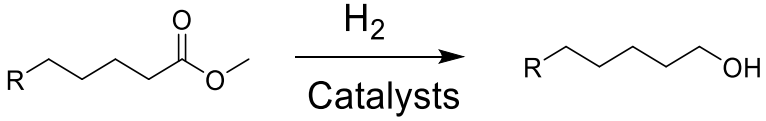

Figure 3 Catalytic steps of fatty acids conversion into fatty alcohols

Commercially, chromium based catalysts like copper chromite have been used for the hydrogenation of FAMES into alcohols at high temperatures and hydrogen pressures (200-400 ^{o}C and 200-300 bar).[13,15] The process is energy intensive due to the transesterification process and high operating conditions for FAMES hydrogenation. This has motivated researchers to develop chromium free catalysts that can directly reduce fatty acids/ fatty acid esters into alcohols. Different catalysts have been thoroughly studied for this process as shown in Table 1 below:

Table 1 Experimental conditions of fatty alcohol production reported by different literatures

Catalysts	Substrate	Experimental conditions	References
Cu-B-SiO_2	esters	240°C, 110 bar H_2	16
Ru-Sn-Al_2O_3	acids	250 ^{o}C, 50-60 bar H_2	17
ReOx-TiO_2	acids	180-200 ^{o}C, 20-40 bar H_2	18
Pt-TiO_2	acids	130°C, 20 bar H_2	19

Despite the success in the selective reduction of acid/esters into alcohols, there is always the need of achieving the conversion under milder conditions, ideally without using noble metals like Ru, Re and Pt. A viable alternative to address this challenge will be presented in Chapter 2.

N-doped ordered mesoporous carbons as catalyst supports

Carbon polymorphs differ from each other in their atomic arrangement (Figure 4).[20] Amorphous carbon is a form of carbon that is primarily composed of graphitic sheetlets with no regular order. Activated carbon, a well-known amorphous carbon, is activated via physical or chemical processes to increase its porosity and hence its surface area.[21] These properties allow activated carbon to be applied in various fields including water purification, catalysis, electrochemistry, gas storage and separations.[21]

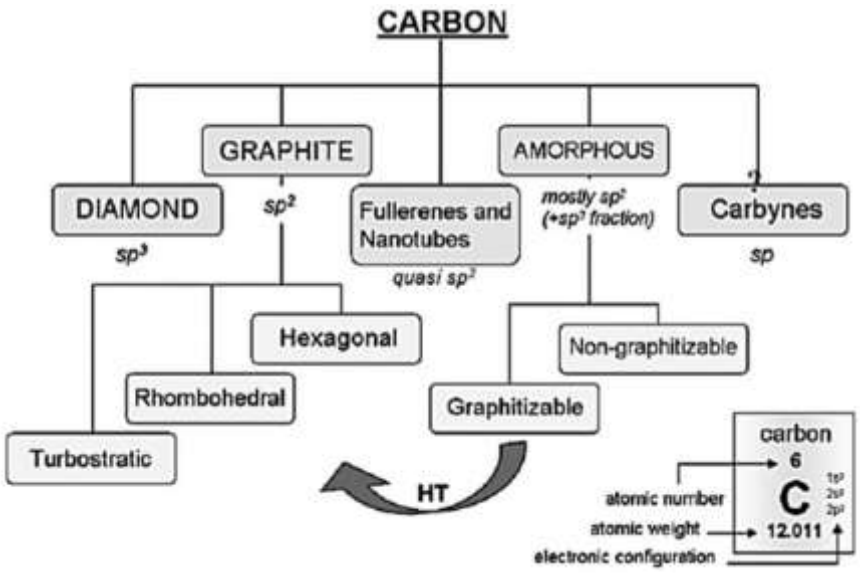

Figure 4 Allotropes of carbon[20]

Porous carbon materials are unique as supports for heterogeneous catalysis owing to the following reasons:[20]

a) Resistance to acidic or basic media

b) Less expensive compared to silica and alumina

c) Hydrothermally stable

d) Active phase can be recovered by combustion of the support

Therefore, development of porous and high surface area carbons is of great importance for various applications.

The nano-casting strategy, also known as hard template method can be used to produce mesoporous carbon as shown in Figure 5. This strategy includes the following steps: a) preparation of a solid template with controlled structure b) infiltration of the template with carbon precursors c) carbonization of the precursors and d) removal of the template. The space previously occupied by the host material becomes the pores and the carbon in the pores of the host becomes the framework in the resulting carbon materials.

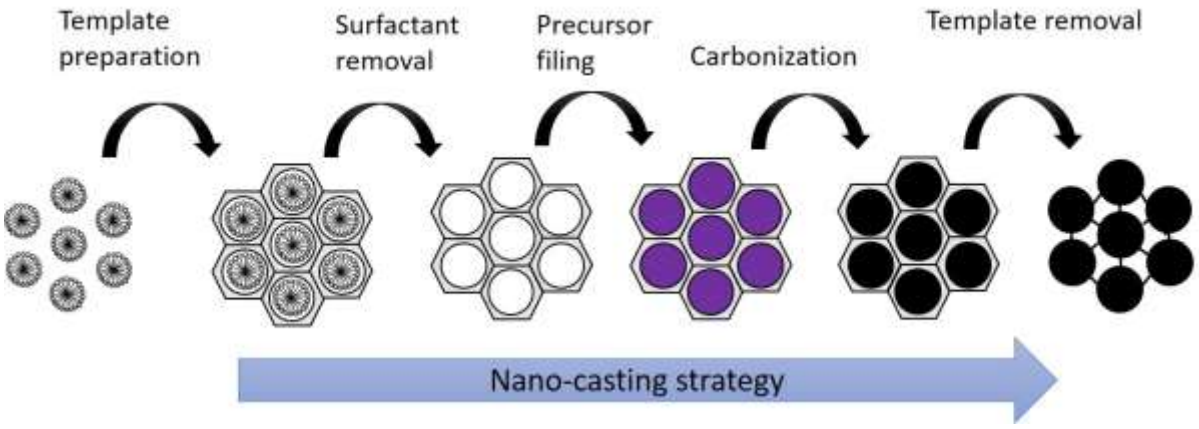

Figure 5 Synthesis of ordered mesoporous carbon[22]

Motivation: Importance of N-containing Carbon

Nitrogen containing carbons are of particular interest in catalysis. Carbons containing basic nitrogen have been reported as catalysts for base catalyzed C-C couplings and transesterification reactions.[23,24] N-doped carbons have also been used as supports for metal catalysts where nitrogen are reported to promote the activity.[25] Similarly, N-doped carbons have been used in other applications like CO_2 capture, improving electro-capacitive properties, and sensing.[26,27, 28] Therefore the development of nitrogen containing mesoporous carbons is of immense importance.

A key challenge of using nano-casting strategy to develop N-doped mesoporous carbons is choosing the most favorable organic precursors.[22] The organic precursors serve as sources for both carbon and nitrogen in the resultant materials. Crosslinking of these precursors is important during carbonization step (Figure 5) because it can help in the formation of continuous carbon framework. Therefore, precursors that can poly-condense under thermal treatment can be favorable for N-doped carbons synthesis. Volatile ionic liquids which decompose below their boiling points have been reported as an attractive alternative for N-doped carbon development.[29,30,31] They can undergo poly-condensation and subsequent aromatization into graphitic structure under thermal treatment. However, ionic liquids are very expensive and they have low yields in carbonization. In Chapter 3 we discuss the development of nitrogen containing mesoporous carbon using biomass-abundant aspartic acid that has the capacity to polymerize at low temperature (200-270 ^{o}C) via hard template method.[32,33]

References

1. Zhao, X. S.; Bao, X. Y.; Guo, W.; Lee, F. Y., Immobilizing catalysts on porous materials. *Materials Today* **2006,** *9* (3), 32-39.
2. Rao, R.; Mishra, B. G., Structural, redoc and catalytic chemistry of ceria based materials. *Bulletin of the catalysis society of India* **2003,** *2*, 122-134.
3. Hayles, J.; Bao, H., The reduction and oxidation of ceria: A natural abundance triple oxygen isotope perspective. *Geochimica et Cosmochimica Acta* **2015,** *159*, 220-230.
4. Vivier, L.; Duprez, D., Ceria-Based Solid Catalysts for Organic Chemistry. *ChemSusChem* **2010,** *3* (6), 654-678.
5. Nelson, N. C.; Manzano, J. S.; Sadow, A. D.; Overbury, S. H.; Slowing, I. I., Selective Hydrogenation of Phenol Catalyzed by Palladium on High-Surface-Area Ceria at Room Temperature and Ambient Pressure. *ACS Catalysis* **2015,** *5* (4), 2051-2061.
6. Si, R.; Raitano, J.; Yi, N.; Zhang, L.; Chan, S.-W.; Flytzani-Stephanopoulos, M., Structure sensitivity of the low-temperature water-gas shift reaction on Cu–CeO2 catalysts. *Catalysis Today* **2012,** *180* (1), 68-80.
7. Tabakova, T.; Boccuzzi, F.; Manzoli, M.; Sobczak, J. W.; Idakiev, V.; Andreeva, D., A comparative study of nanosized IB/ceria catalysts for low-temperature water-gas shift reaction. *Applied Catalysis A: General* **2006,** *298* (0), 127-143.
8. Sakata, Y.; Ponec, V., Reduction of benzoic acid on CeO2 and, the effect of additives. *Applied Catalysis A: General* **1998,** *166* (1), 173-184.
9. Rao, K. N.; Bharali, P.; Thrimurthulu, G.; Reddy, B. M., Supported copper–ceria catalysts for low temperature CO oxidation. *Catalysis Communications* **2010,** *11* (10), 863-866.
10. Zheng, X.; Wang, S.; Wang, S.; Zhang, S.; Huang, W.; Wu, S., Copper oxide catalysts supported on ceria for low-temperature CO oxidation. *Catalysis Communications* **2004,** *5* (12), 729-732.
11. Holmberg, K., Natural surfactants. *Current Opinion in Colloid & Interface Science* **2001,** *6* (2), 148-159.
12. Gupta, S., Dynamics of the global fatty alcohol market. Frost and Sullivan market insight: 2004.
13. Voeste, T.; Buchold, H., Production of fatty alcohols from fatty acids. *Journal of the American Oil Chemists' Society* **1984,** *61* (2), 350-352.
14. Kandel, K.; Anderegg, J. W.; Nelson, N. C.; Chaudhary, U.; Slowing, I. I., Supported iron nanoparticles for the hydrodeoxygenation of microalgal oil to green diesel. *Journal of Catalysis* **2014,** *314*, 142-148.
15. Rieke, R.; Thakur, D.; Roberts, B.; White, G., Fatty methyl ester hydrogenation to fatty alcohol part II: Process issues. *Journal of the American Oil Chemists' Society* **1997,** *74* (4), 341-345.
16. Chen, Y. Z.; Chang, C. L., Cu-B2O3/SiO2, an effective catalyst for synthesis of fatty alcohol from hydrogenolysis of fatty acid esters. *Catalysis Letters* **1997,** *48* (1-2), 101-104.
17. Toba, M.; Tanaka, S.-i.; Niwa, S.-i.; Mizukami, F.; Koppány, Z.; Guczi, L.; Cheah, K.-Y.; Tang, T.-S., Synthesis of alcohols and diols by hydrogenation of carboxylic acids and esters over Ru–Sn–Al2O3 catalysts. *Applied Catalysis A: General* **1999,** *189* (2), 243-250.

18. Rozmysłowicz, B.; Kirilin, A.; Aho, A.; Manyar, H.; Hardacre, C.; Wärnå, J.; Salmi, T.; Murzin, D. Y., Selective hydrogenation of fatty acids to alcohols over highly dispersed ReOx/TiO2 catalyst. *Journal of Catalysis* **2015,** *328*, 197-207.
19. Manyar, H. G.; Paun, C.; Pilus, R.; Rooney, D. W.; Thompson, J. M.; Hardacre, C., Highly selective and efficient hydrogenation of carboxylic acids to alcohols using titania supported Pt catalysts. *Chemical Communications* **2010,** *46* (34), 6279-6281.
20. Lam, E.; Luong, J. H. T., Carbon Materials as Catalyst Supports and Catalysts in the Transformation of Biomass to Fuels and Chemicals. *ACS Catalysis* **2014,** *4* (10), 3393-3410.
21. Carbon (Nano)materials for Catalysis. In *Nanostructured Carbon Materials for Catalysis*, The Royal Society of Chemistry: 2015; pp 1-45.
22. Ma, T.-Y.; Liu, L.; Yuan, Z.-Y., Direct synthesis of ordered mesoporous carbons. *Chemical Society Reviews* **2013,** *42* (9), 3977-4003.
23. Villa, A.; Tessonnier, J.-P.; Majoulet, O.; Su, D. S.; Schlögl, R., Transesterification of Triglycerides Using Nitrogen-Functionalized Carbon Nanotubes. *ChemSusChem* **2010,** *3* (2), 241-245.
24. Kan-nari, N.; Okamura, S.; Fujita, S.-i.; Ozaki, J.-i.; Arai, M., Nitrogen-Doped Carbon Materials Prepared by Ammoxidation as Solid Base Catalysts for Knoevenagel Condensation and Transesterification Reactions. *Advanced Synthesis & Catalysis* **2010,** *352* (9), 1476-1484.
25. Jagadeesh, R. V.; Surkus, A. E.; Junge, H.; Pohl, M. M.; Radnik, J.; Rabeah, J.; Huan, H.; Schunemann, V.; Bruckner, A.; Beller, M., Nanoscale Fe_2O_3-based catalysts for selective hydrogenation of nitroarenes to anilines. *Science* **2013,** *342* (6162), 1073-1076.
26. Cayuela, A.; Carrillo-Carrión, C.; Soriano, M. L.; Parak, W. J.; Valcárcel, M., One-Step Synthesis and Characterization of N-Doped Carbon Nanodots for Sensing in Organic Media. *Analytical Chemistry* **2016**.
27. Lei, Z.; Bai, D.; Zhao, X. S., Improving the electrocapacitive properties of mesoporous CMK-5 carbon with carbon nanotubes and nitrogen doping. *Microporous and Mesoporous Materials* **2012,** *147* (1), 86-93.
28. Bandosz, T. J.; Seredych, M.; Rodríguez-Castellón, E.; Cheng, Y.; Daemen, L. L.; Ramírez-Cuesta, A. J., Evidence for CO2 reactive adsorption on nanoporous S- and N-doped carbon at ambient conditions. *Carbon* **2016,** *96*, 856-863.
29. Paraknowitsch, J. P.; Thomas, A.; Antonietti, M., A detailed view on the polycondensation of ionic liquid monomers towards nitrogen doped carbon materials. *Journal of Materials Chemistry* **2010,** *20* (32), 6746-6758.
30. Zhang, S.; Miran, M. S.; Ikoma, A.; Dokko, K.; Watanabe, M., Protic Ionic Liquids and Salts as Versatile Carbon Precursors. *Journal of the American Chemical Society* **2014,** *136* (5), 1690-1693.
31. Lim, K. H.; Kim, H., Nitrogen-doped carbon catalysts derived from ionic liquids in the presence of transition metals for the oxygen reduction reaction. *Applied Catalysis B: Environmental* **2014,** *158–159*, 355-360.
32. Nakato, T.; Kusuno, A.; Kakuchi, T., Synthesis of poly(succinimide) by bulk polycondensation of L-aspartic acid with an acid catalyst. *Journal of Polymer Science Part A: Polymer Chemistry* **2000,** *38* (1), 117-122.
33. Wang, Y.; Hou, Y.; Zhang, J.; Ruan, G., Kinetics of dehydration–polymerization of aspartic acid and synthesis of polyaspartate catalyzed by potassium bisulfate. *Polymer International* **2004,** *53* (2), 156-162.

CHAPTER 2

INVESTIGATIONS ON HYDROGENATION OF FATTY ACIDS INTO FATTY ALCOHOLS USING COPPER OXIDE CATALYSTS SUPPORTED ON CERIA

Abstract: Copper oxide supported on ceria has been investigated for the selective hydrogenation of octadecanoic acid to octadecanol. At reaction conditions of 5 bar H_2 at 250 ^oC, 75 % alcohol yield with 100 % selectivity can be achieved. The Cu^o species formed under the experimental conditions and ceria support likely show synergy for the selective hydrogenation of acids into alcohols.

Introduction

Fatty alcohols are industrially important as they are used as raw materials in emulsifiers, thickeners, lubricants, plasticizers, solvents, alternative fuels and cosmetics.[1] The current world production capacity of fatty alcohols reaches 3.35 Mt/a with an estimated global demand growth (2012-2017) of 3.2 %/a.[2] Due to the decrease in fossil fuel resources and increase in consumer demand, bio-renewable feedstocks rich in fatty acids are thoroughly studied for producing fatty alcohols.[3] Catalytic hydrogenation is an important method for transforming fatty acids, methyl esters or wax esters into the corresponding fatty alcohols.[4] In the conventional technology, the production of fatty alcohols involves methanolysis of triglycerides or fatty acids, followed by hydrogenolysis using copper chromite or zinc chromite based catalysts at high temperatures (200°C - 400°C) and hydrogen pressures (200 - 300 bar).[5] As a result, there is a pressing need for the development of alternative chromium free catalysts to selectively convert fatty acids/esters into fatty alcohols at lower pressures and temperatures.

Investigations on chromium free catalysts have been reported by Chang and co-workers where they have shown the hydrogenolysis of their methyl esters into alcohols using Cu-B_2O_3/SiO_2 catalyst at 240°C and 110 bar H_2.[6] Direct reduction of fatty acids into alcohols is more fascinating as it avoids the transesterification step. Investigations using ruthenium based catalysts like ruthenium supported on carbon (60 bar H_2, 100 ^oC), ruthenium heptaoxide (250-350 bar H_2, 150-200 ^oC), ruthenium-tin supported on alumina (50-60 bar H_2, 250 ^oC), and ruthenium oxide supported on titania (220 ^oC, 40 bar H_2) catalysts among others have been reported.[7, 8] Recently, highly dispersed ReO_x/TiO_2 catalyst has also been reported by Dmitry et al. for the selective hydrogenation of fatty acids into alcohols at temperatures and pressures between 180-200 ^oC and 20-40 bar H_2 respectively.[9] Similarly, Hardacre and his group demonstrated acid to alcohol conversion using Pt/TiO_2 catalysts at much milder reaction conditions (130°C and 20 bar H_2) but the reaction time was 12 h for 82 % conversion).[10] These results are remarkable. However, it is desirable to replace the expensive noble metals with catalysts containing more inexpensive metals still capable of selective reduction of acids into alcohols at much lower hydrogen pressures (ideally close to 1 bar).

Many groups have reported the significance of bimetallic composite catalysts for the hydrogenation of fatty acids into fatty alcohols.[8,10] Recently we have shown that Cu and Fe oxides supported on silica synergistically hydrogenate fatty acids to fatty alcohols at milder conditions (180 ^oC and 30 bar H_2) compared to individual supported metal oxides.[11] We have shown that designing a composite catalyst that contains both H_2 activation metal centers and acid activation metal oxide centers can significantly lower the experimental conditions for hydrogenation reactions. With this insight in mind, we chose to combine cerium dioxide (ceria) and copper oxide as a composite catalyst. Copper oxide supported on ceria is widely

reported in enhancement of the activity and selectivity of ceria-based redox catalysts, because incorporation of copper species onto ceria supports are known to enhance oxygen diffusion and reducibility of ceria.[12,13,14] Similarly, reports have shown ceria as an active hydrogenation catalyst.[15,16,17] However, investigations on direct reduction of acids to alcohols using ceria based catalysts are still lacking. The majority of studies using ceria-based catalysts are focused on three-way catalytic converters, fluid catalytic cracking and oxidation reactions.[18] In this work, copper oxide supported on ceria (CuO/CeO_2) catalysts are investigated for the first time, to the best of our knowledge, for the direct hydrogenation of fatty acid into fatty alcohol. This work demonstrates the selective conversion of octadecanoic acid (stearic acid; a model fatty acid) into octadecanol (stearyl alcohol) using earth abundant copper and redox active ceria as a composite catalyst at low H_2 pressure.

Experimental Section

Reagents

Cerium (III) nitrate hexahydrate ($Ce(NO_3)_3 \cdot 6H_2O$), Copper (II) nitrate hemi (pentahydrate) ($Cu(NO_3)_2 \cdot 2.5H_2O$) were purchased from Sigma Aldrich. Pluronic P104 and Pluronic P123 were obtained from BASF. Ethanol (100%) was used for the catalyst synthesis. All chemicals were used as received without further purification.

Synthesis of Ceria (CeO_2)

CeO_2 was synthesized by previously reported procedure developed by our group.[19] In a typical synthesis, $Ce(NO_3)_3 \cdot 6H_2O$ (8.80 g, 20.3 mmol) and Pluronic P104 (10.1 g, 1.71 mmol) were dissolved in ethanol (200 mL) with vigorous stirring for 3 h. The solution was then cast into a large crystallization dish and placed into a preheated 65 °C oven to undergo

solvent evaporation. After 24 h, the gel was placed into an oven preheated to 150 °C for additional 12 h. The material was then further calcined at 450 °C for 4 h with a ramp rate of 1 °C min^{-1}.

Synthesis of Ceria supported Copper Oxide catalysts (CuO/CeO_2)

CuO/CeO_2 catalysts were prepared by incipient wetness impregnation. Different amounts of $Cu(NO_3)_2$•$2.5H_2O$ were dissolved in acetone under sonication for 15 minutes and added to ceria drop by drop followed by grinding with mortar and pestle. The mixture was dried at 60 ^oC for 3 h followed by calcination at 350 ^oC, for 6 h with a ramp rate of 2 ^oC min^{-1}. These catalysts were labeled based on the mole ratio of Cu to that of ceria (calculated using wt % of Cu given by ICP-OES) as shown in **Table** 2 (column 3).

Characterization

Surface areas of CeO_2 and CuO/CeO_2 catalysts were measured by nitrogen sorption isotherms at -196 ^oC in a Micromeritics Tristar analyzer. The surface areas were calculated by the Brunauer−Emmett−Teller (BET) method and the pore volume was calculated by the Barret-Joyner-Halenda (BJH) method. Diffraction patterns were collected using Co Kα1, Kα2 split radiation (45 kV, 40 mA, λavg = 1.7903 Å) on a PANalytical X'Pert PRO diffractometer. The spectra were converted to Cu Kα radiation for comparison to standard patterns. ICP-OES was used to measure Cu content present on the ceria support. Samples for ICP measurements were prepared by digesting CuO/CeO_2 catalysts (5 mg) in 10 ml of aqueous HF and HCl solution (0.18 and 5 v/v %, respectively). Hydrogen temperature-programmed reduction (H_2-TPR) experiments were performed in a Micromeritics AutoChem II instrument using H_2 in Ar (H_2/Ar) (10.1 %) as the reducing agent. Typically, 30 mg of

catalyst was used for TPR analysis. Samples were placed in U-tube sample holder and pretreated in situ by heating at 350 ^{o}C for 1 hr followed by cooling down to ambient temperature. Then immediately, H_2 consumption by the samples were measured by flowing of H_2/Ar (50 mL min^{-1}) with a ramp rate of 10 ^{o}C min^{-1} from ambient temperature to 800 ^{o}C. A cold trap (dry ice in acetone) was used to collect water produced during the reduction. XPS analysis was done using PHI 5500 multitechnique system with a standard Al X-Ray source, charge correction was done using O_{1S} peak at 529.0 eV for all spectra. Transmission electron microscopy (TEM) and scanning transmission electron microscopy (STEM) studies on the materials were done using Tecnai G2 F29 electron microscope operated at 200 kV. Elemental mapping and energy dispersive X-ray spectroscopy (EDS) in STEM mode were used to characterize the spatial composition of the material. To prepare the samples for these studies, materials (5 mg) were suspended in 5 ml of ethanol, sonicated for 30 minutes and finally 3-4 drops of suspensions were placed onto lacey-carbon-coated gold grids.

Catalytic activity measurement

All catalytic reactions were performed in a 100-mL batch reactor (Parr Instruments). In a typical experiment, the catalyst (10 mg) and stearic acid solution in hexanes (10 mM, 10 mL) were added to the reactor. The reactor was purged with H_2 and then pressurized with H_2 at ambient temperature. In order to optimize the reaction conditions, the reaction was carried out at various temperatures or pressures for 2 h with a stir rate of 500 rpm. For kinetics study, the reaction was carried out separately for different time intervals. The reaction products were derivatized using Sylon BFT at 70 ^{o}C for 1 h and analyzed in an Agilent GC-MS (7890A, 5975C) with a HP–5MS column using 1-methyl nonadecanoate as an internal standard. Conversion was calculated as moles of converted stearic acid per moles of starting

stearic acid times 100 % and yields were calculated as moles of each product per moles of starting stearic acid times 100%.

Results and Discussions

Catalysts Characterization

The textural properties of CeO_2 and CuO/CeO_2 catalysts and their composition are summarized in Table 2. N_2 sorption analysis showed the high surface area of the ceria support. ICP measurements were done to calculate the amount of Cu present on ceria. The surface area and pore volume of the CuO/CeO_2 catalysts decreased steadily with increasing loadings of Cu. To study the nature of Cu species and crystalline phases of CuO/CeO_2 catalysts, the as-prepared materials were characterized by wide-angle x-ray diffraction. As shown in Figure 6, all the samples showed reflections at 2 theta of 28.8º, 33.3º, 47.9º and 56.8º, attributed to the fluorite cubic structure of ceria (JCPDS 34-0394).[20] On the other hand, no diffraction peaks attributed to CuO were present for CuO/CeO_2 catalysts until the Cu loading reached to 7.9 wt. %, indicating that CuO on ceria surface might be amorphous, highly dispersed or forming crystallites smaller than the detection limit of the instrument (<2 nm). EDS elemental mapping of 0.056 Cu/CeO_2 catalyst confirmed that copper was well dispersed on the ceria support (Figure 7). The oxidation state of copper was confirmed as 2+ by XPS analysis of 2.0 wt % Cu containing CuO/CeO_2 catalyst (Figure 8) which is consistent with XRD result of higher loaded CuO/CeO_2 catalyst.[21] Further XPS analysis of Ce (3d) exhibited $3d_{5/2}$ and $3d_{3/2}$ peaks at 881 eV and 900 eV respectively along with satellite peaks confirming the oxidation state of cerium as Ce^{4+} in the copper ceria catalyst.[21]

Table 2 Textural properties and the composition of CeO_2 support and CuO/CeO_2 catalysts

Cu wt% [a]	Cu mmol/g	CuO/CeO_2 mole ratio	Surface area (m^2/g) [b]	Pore volume (cm^3/g) [b]
0	0	0	212	0.274
0.65	0.10	0.018	195	0.259
2.0	0.32	0.056	180	0.253
4.4	0.69	0.12	151	0.219
7.9	1.2	0.23	135	0.182

[a]Obtained by ICP-OES. [b]Obtained by N_2 sorption isotherms

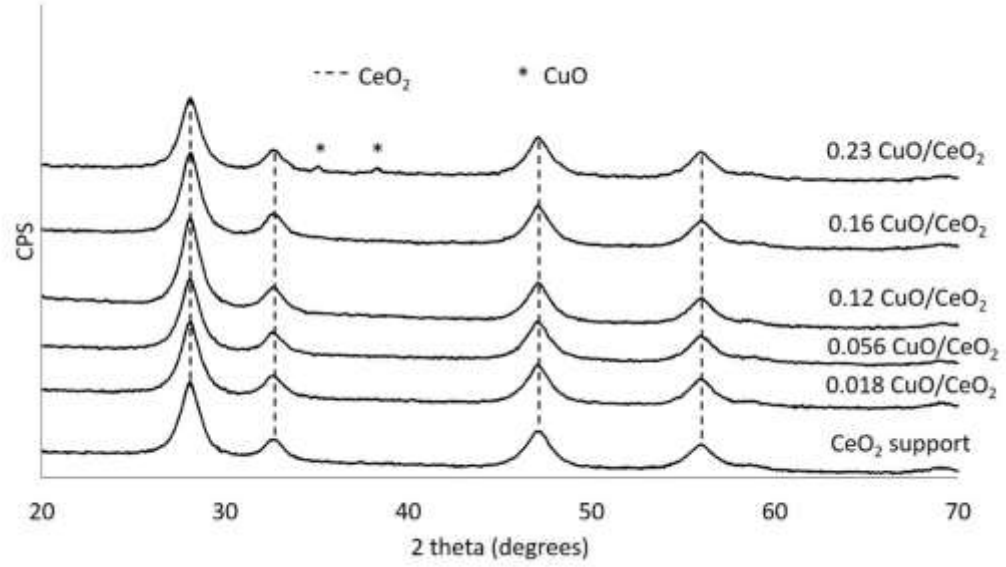

Figure 6 Wide angle XRD patterns of CeO_2 and CuO/CeO_2 catalysts

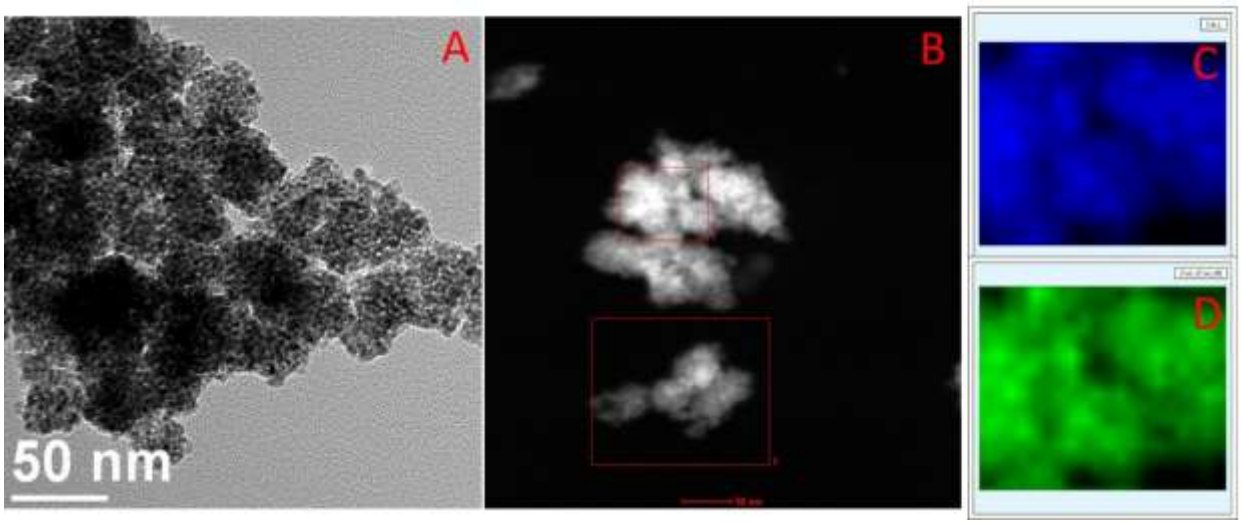

Figure 7 A) TEM B) STEM images and C) and D) EDS maps of 0.056 CuO/CeO_2 catalyst. Maps correspond to C) cerium and D) copper.

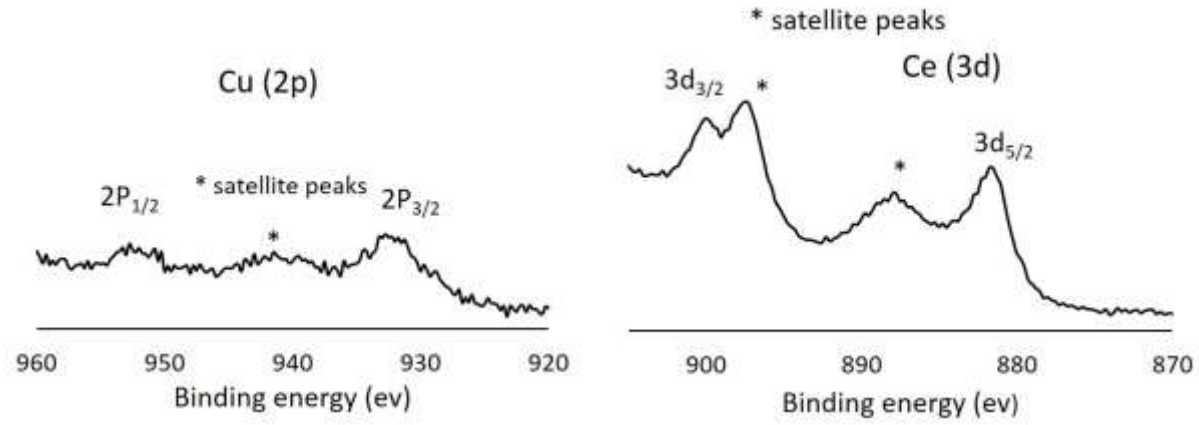

Figure 8 XPS of Cu (2p) and Ce (3d) in 0.056 CuO/ CeO_2

H_2-TPR was carried out on CuO, CeO_2 and CuO-CeO_2 catalysts in order to investigate the reducibility of the materials. H_2-TPR of ceria support showed hydrogen consumption at 415 ^oC and 646 ^oC which are attributed to surface ceria reduction and bulk ceria reduction, respectively (Figure 9A).[13] Also a control experiment involving H_2-TPR of bulk CuO showed reduction peaks at 286 ^oC and 443 ^oC (Figure 9A). Upon deposition of copper precursor and calcination in air, the hydrogen consumption profile changed drastically from that of CeO_2 (Figure 9B). The peak at 415 °C was no longer present, while two new

peaks emerged below 150 °C, depending on the copper loading. This indicates the copper ceria composite catalysts are redox active below 150 ^{o}C. Previous reports have attributed the reduction peak at lower temperature (~129 ^{o}C) to highly dispersed CuO interacting with ceria while the reduction at higher temperature (~141 ^{o}C) has been attributed to larger CuO particle interacting with ceria.[22, 23] Based on the amounts of Cu loaded on ceria, the theoretical H_2 consumption for the transformation of Cu^{2+} to Cu^{0} were calculated and compared to the H_2 consumption by copper-ceria catalysts. Our results showed the actual experimental H_2 consumption by copper-ceria catalysts was larger than the amount of H_2 needed to fully reduce CuO to Cu^{0} (Table 3). This fact, together with the disappearance of peak at 415 ^{o}C present in ceria may indicate the excess hydrogen was used to remove the reducible oxygen present on the surface layer of ceria on the support or remained physisorbed on the support.[13]

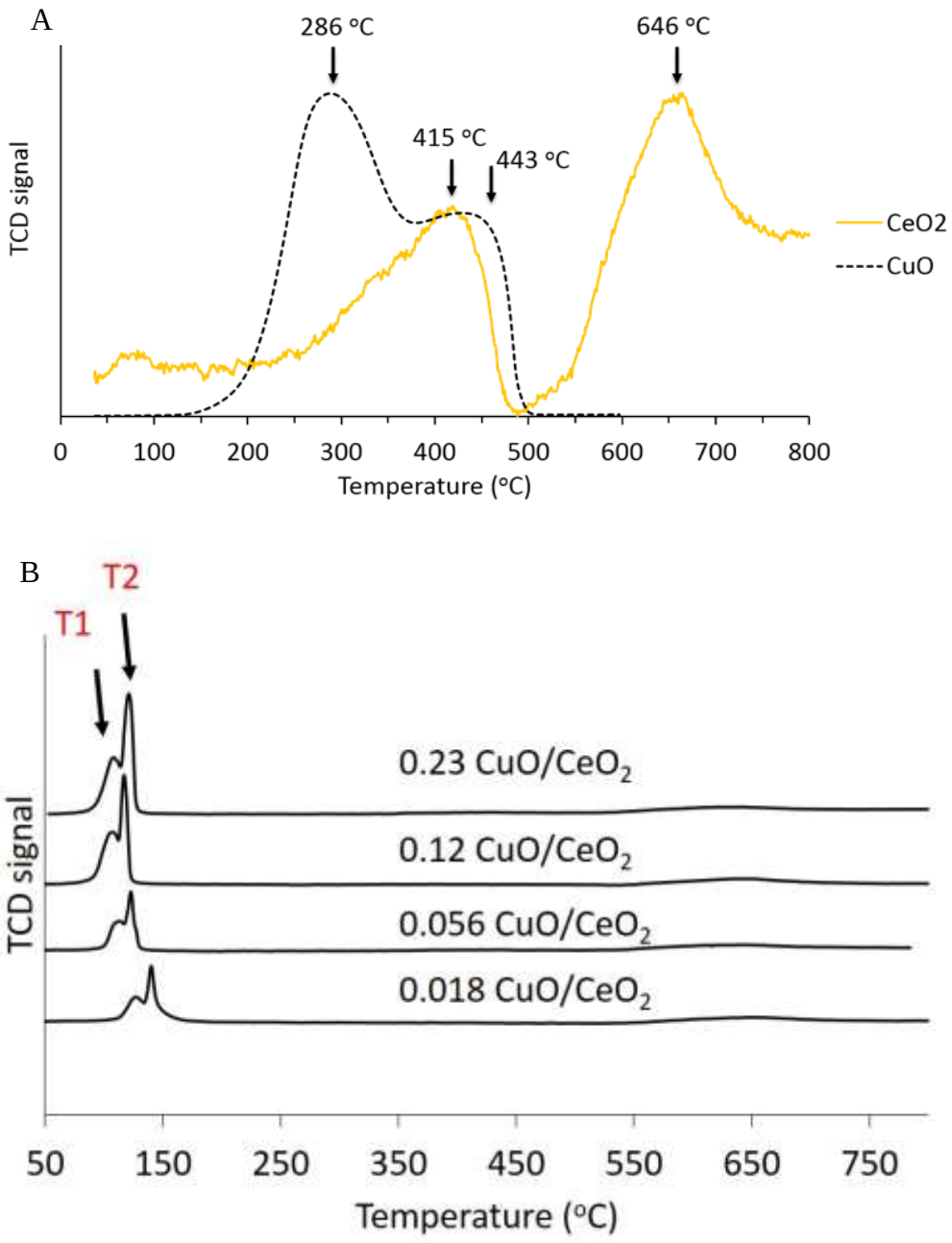

Figure 9 H2-TPR of A) CuO (black) and Ceria (yellow) B) CuO-CeO_2 catalysts

Table 3 Hydrogen consumption of as-prepared CeO_2 and CuO/CeO_2 catalysts by H_2-TPR

Catalysts	H_2 consumption (mmol/g)					
	at T1	at T2	total at (T1+T2)	Theoretical for CuO to Cu(0)[a]	T1 (^oC)	T2 (^oC)
0.018 CuO/CeO2	0.73	0.24	0.97	0.10	129	141
0.056 CuO/CeO_2	0.95	0.44	1.39	0.32	112	124
0.12 CuO/CeO_2	1.23	0.79	2.01	0.69	107	117
0.23 CuO/CeO_2	0.75	1.38	2.13	1.23	105	121

[a]Based on Cu in the sample measured by ICP-OES.

Activity of Ceria Support

The ceria support was tested for hydrogenation of octadecanoic acid at variable temperatures using 30 bar H_2 for 3h (Figure 10). Ceria was inactive below 200 ^oC, but showed slight activity at 230 ^oC (9 % conversion). As the temperature was increased to 250 ^oC, the conversion of octadecanoic acid increased to 78 %. Octadecanal was the main product obtained with 91 % selectivity at this condition (250 ^oC, 30 bar, 3h). These results are consistent with the studies done by Sakata et al. on gas phase reactions of aromatic acids over ceria.[15] They have reported the reduction of benzoic acid on CeO_2 in a flow reactor at reaction conditions of 250 ^oC – 450 ^oC and total hydrogen pressure of 1 bar H_2. Under these conditions, they observed the 95 % selectivity to benzaldehyde as a product and they reported that the activity was controlled by the number of oxygen vacancies. Further, we tested the hydrogenation at different pressures (5 bar and 30 bar) at 250 ^oC for 2 h to study the hydrogen amount effect on the catalytic activities. As shown in Figure 11, the results suggest that the activity of the ceria support is pressure dependent.

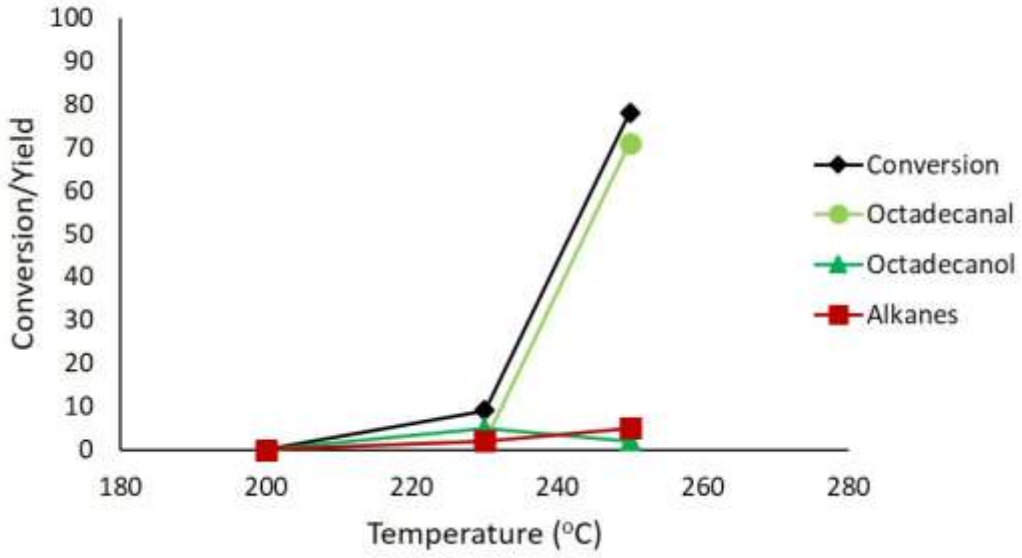

Figure 10 Hydrogenation activity of CeO_2 support (Conditions: 10 mM, 10 mL Octadecanoic acid, 30 bar H_2, 3h)

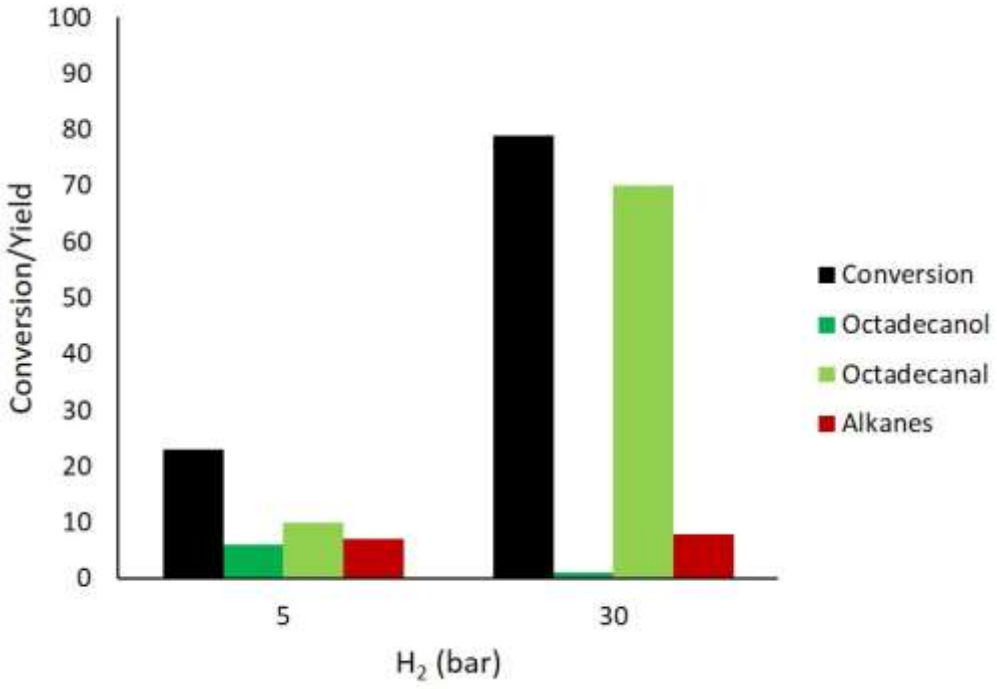

Figure 11 Hydrogenation activity of CeO_2 support (Conditions: 10 mM, 10 mL Octadecanoic acid, 250 ºC, 2h)

To study the effect of reaction time on product distribution, hydrogenations of octadecanoic acid using ceria as catalyst were performed at different reaction times at 250 ^{o}C, 30 bar H_2 as shown in Figure 12. At 0.5 h of reaction time, 60 % conversion of octadecanoic acid was observed. As the reaction time was increased, the conversion also increased. The yield and selectivity of octadecanal also increased with the increase in reaction time. Moreover, the selectivity of alkanes stayed almost same (less than 9 %).

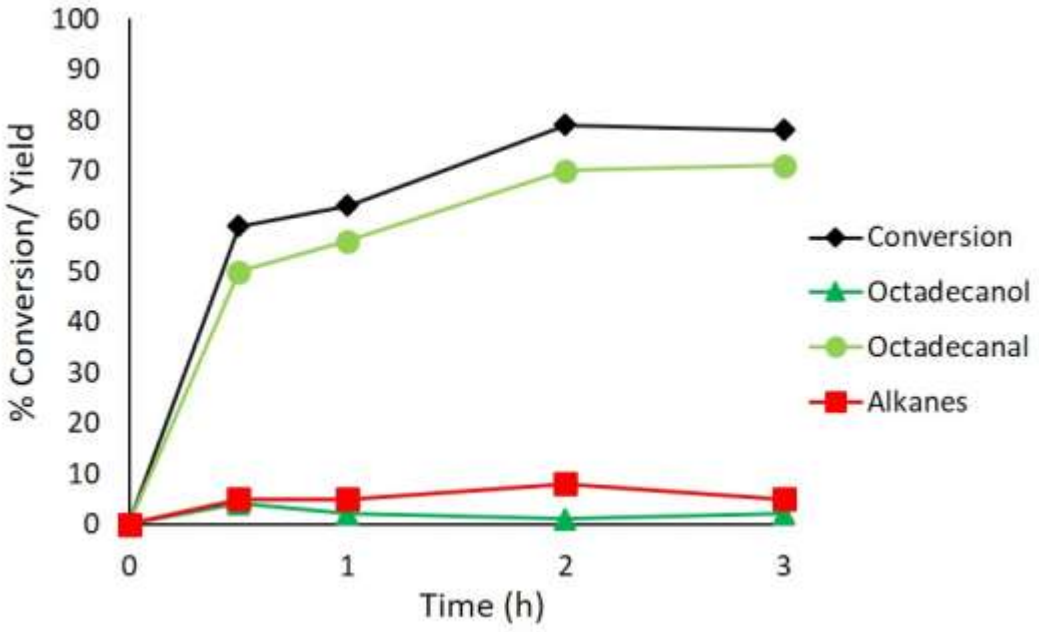

Figure 12 Hydrogenation activity of CeO_2 support (Conditions: 10 mM, 10 mL Octadecanoic acid, 250 ^{o}C, 30 bar H_2)

Activity of CuO/CeO_2 Catalysts

A series of CuO/CeO_2 catalysts containing different amounts of Cu were tested for hydrogenation of octadecanoic acid at 250 ^{o}C, 5 bar H_2, 2 h as shown in Figure 13. The results showed that the addition of copper to ceria affects the hydrogenation activity. We have shown above that ceria is an active hydrogenation catalyst at 250 ^{o}C, 30 bar H_2, but as the pressure was lowered from 30 bar to 5 bar H_2 (both at 250 ^{o}C, 2 h), the conversion went

down from 80 % to 23 %. However all CuO/CeO_2 catalysts showed higher % octadecanoic conversion than CeO_2 alone at 5 bar (Figure 13). Interestingly, the amount of Cu supported on ceria affects the product selectivities: the higher the amount of Cu in ceria, the more the selectivity to alkanes. This may result from the high storage of H_2 in CuO/CeO_2 catalysts with higher Cu loading as indicated by quantitative H_2 consumption results from TPR (Table 3). This spilled over H_2 may be used for further reduction of alcohols formed during reaction to the alkanes.

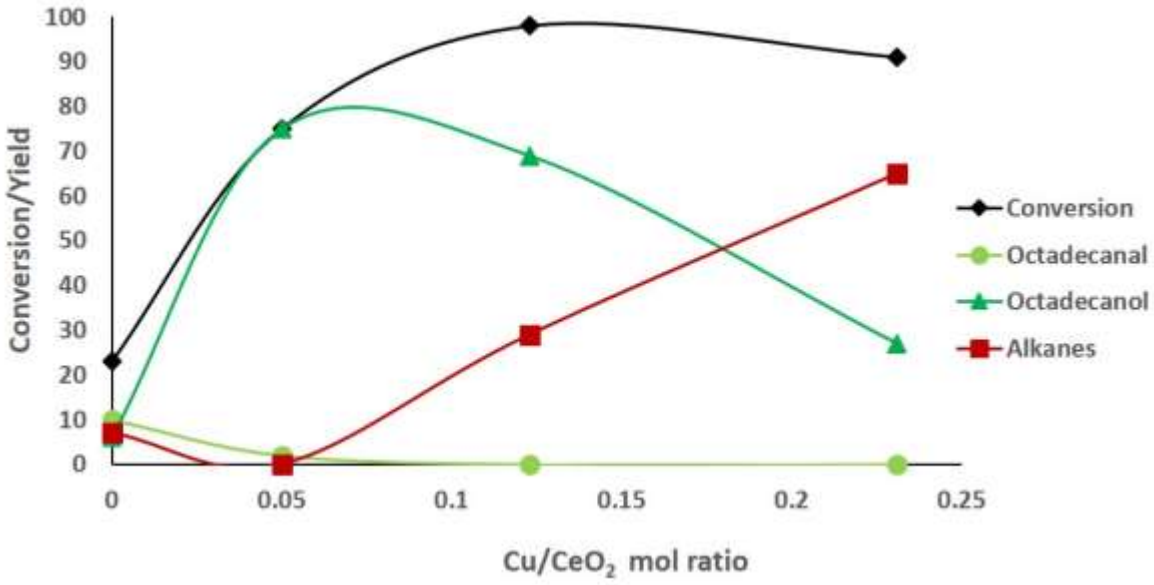

Figure 13 Hydrogenation activity of CuO-CeO_2 catalysts (Conditions: 10 mM, 10 mL Octadecanoic acid, 250 ^oC, 5 bar H_2, 2 h)

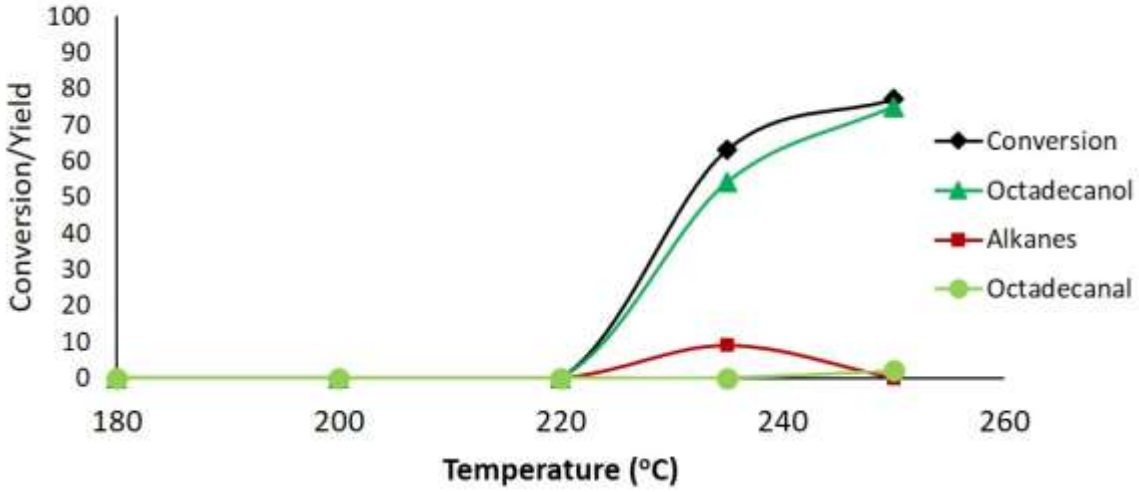

Figure 14 Hydrogenation activity of 0.056 CuO-CeO_2 (Conditions: 10 mM, 10 mL Octadecanoic acid, 5 bar H_2, 2 h)

The 0.056 CuO/CeO_2 catalysts showed 100 % octadecanol selectivity at 250 ^oC, 5 bar H_2. Therefore this catalyst was further used for screening hydrogenation activities at 5 bar H_2 pressure for 2 h at varying temperatures as shown in Figure 14. The light off curve plot shows the catalyst is active above 220 ^oC.

Active Sites in CuO-CeO_2 Catalysts

To determine the active species of the copper-ceria catalysts a series of control reactions were performed at 250 ^oC, 5 bar H_2 for 2 h. While bare ceria gave 23 % conversion of acid to aldehyde, CuO nanoparticles did not show any catalytic activity for hydrogenation under the same reaction conditions. Also, hydrogenation of stearic acid with a physical mixture of ceria and CuO gave only 18 % conversion. These results clearly show synergy between CuO and ceria in CuO/CeO_2 catalysts for the reaction.

To identify the phases of Cu and Ce in the catalyst, H_2-TPR experiments of 0.231 CuO/CeO_2 material were performed followed by XRD analysis (Figure 15). The reduction was stopped at 125 ^oC and 150 ^oC (temperatures after peak 1 and peak 2 in Figure 7B) in the respective experiments. The XRD patterns (Figure 15) clearly indicate a loss of CuO crystalline phase at 125 °C, however no other phase that could be assigned to copper species is observed after this temperature. Upon heating to 150 °C the formation of metallic Cu can be appreciated from the XRD pattern. This transformation of Cu^{2+} into Cu^o in our composite catalyst under reducing environment is consistent with the work reported by Zhu et al.[24] The presence of Cu in ceria facilitates the reduction of Ce^{4+} (Figure 9B) and oxygen vacancies are most likely created close to the support interface with metal nanoparticles.[25,26] These data may suggest the metallic Cu and oxygen vacancies created under the reaction conditions may work as such an ensemble of active centers. The in situ generated metallic Cu most likely activates H_2 which is transferred to reduce the acids activated on oxygen vacancies.[11]

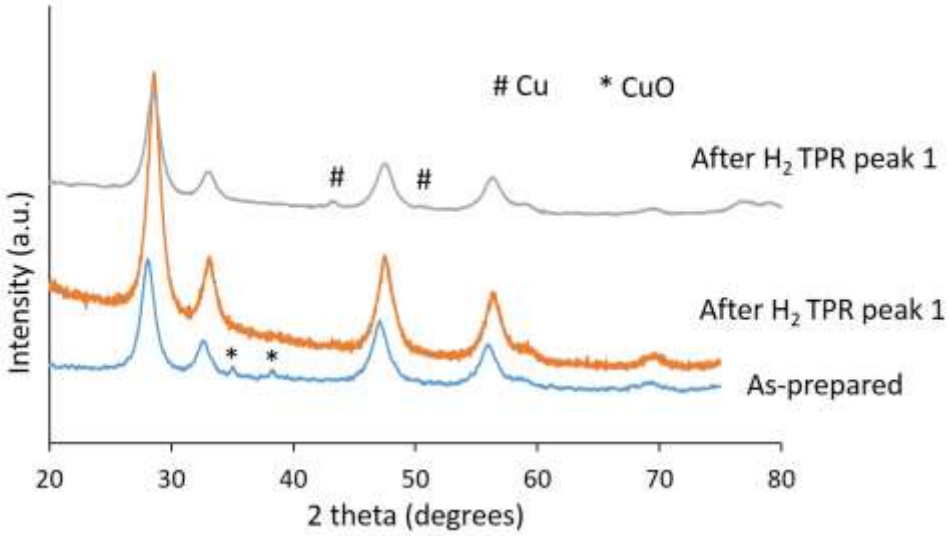

Figure 15 Wide angle XRD patterns of a) as-prepared b) reduced at 125 ^oC c) reduced at 150 ^oC 0.231 CuO/CeO_2 catalyst

Conclusions

CuO supported ceria catalysts have shown promising results for the direct hydrogenation of octadecanoic acid into octadecanol at low pressure (5 bar). Synergistic interaction between CuO and ceria nanoparticles plays a crucial role on the hydrogenation activity where reduced copper and oxygen vacancies created during the reaction conditions are likely the active sites. The selectivity to alkanes can be further tuned by increasing the amount of Cu on the ceria support.

References

1. Holmberg, K., Natural surfactants. *Current Opinion in Colloid & Interface Science* **2001,** *6* (2), 148-159.
2. Clay, B., Detergent Alcohols: Growing Capacity Will Continue to Drive down Operating Rates. 2013.
3. Christensen, C. H.; Rass-Hansen, J.; Marsden, C. C.; Taarning, E.; Egeblad, K., The Renewable Chemicals Industry. *ChemSusChem* **2008,** *1* (4), 283-289; Pfaltzgraff, L. A.; De bruyn, M.; Cooper, E. C.; Budarin, V.; Clark, J. H., Food waste biomass: a resource for high-value chemicals. *Green Chemistry* **2013,** *15* (2), 307-314; Metzger, J. O.; Bornscheuer, U., Lipids as renewable resources: current state of chemical and biotechnological conversion and diversification. *Applied Microbiology and Biotechnology* **2006,** *71* (1), 13-22; Meier, M. A. R.; Metzger, J. O.; Schubert, U. S., Plant oil renewable resources as green alternatives in polymer science. *Chemical Society Reviews* **2007,** *36* (11), 1788-1802.
4. Uccinai, E., *Heterogeneous catalysis and fine chemicals*. Elsevier: Amsterdam, 1988.
5. Voeste, T.; Buchold, H., Production of fatty alcohols from fatty acids. *Journal of the American Oil Chemists' Society* **1984,** *61* (2), 350-352; Rieke, R.; Thakur, D.; Roberts, B.; White, G., Fatty methyl ester hydrogenation to fatty alcohol part II: Process issues. *Journal of the American Oil Chemists' Society* **1997,** *74* (4), 341-345; Kreutzer, U., Manufacture of fatty alcohols based on natural fats and oils. *Journal of the American Oil Chemists' Society* **1984,** *61* (2), 343-348; Turek, T.; Trimm, D. L.; Cant, N. W., The Catalytic Hydrogenolysis of Esters to Alcohols. *Catalysis Reviews* **1994,** *36* (4), 645-683.
6. Chen, Y. Z.; Chang, C. L., Cu-B2O3/SiO2, an effective catalyst for synthesis of fatty alcohol from hydrogenolysis of fatty acid esters. *Catalysis Letters* **1997,** *48* (1-2), 101-104.
7. Carnahan, J. E.; Ford, T. A.; Gresham, W. F.; Grigsby, W. E.; Hager, G. F., Ruthenium-catalyzed Hydrogenation of Acids to Alcohols. *Journal of the American Chemical Society* **1955,** *77* (14), 3766-3768; Guyer, A.; Bieler, A.; Jaberg, K., Über die katalytische Reduktion der Carboxylgruppe aliphatischer Säuren. *Helvetica Chimica Acta* **1947,** *30* (1), 39-43; Broadbent, H. S.; Campbell, G. C.; Bartley, W. J.; Johnson, J. H., Rhenium and Its Compounds as Hydrogenation Catalysts. III. Rhenium Heptoxide1,2,3. *The Journal of Organic Chemistry* **1959,** *24* (12), 1847-1854; Toba, M.; Tanaka, S.-i.; Niwa, S.-i.; Mizukami, F.; Koppány, Z.; Guczi, L.; Cheah, K.-Y.; Tang, T.-S., Synthesis of alcohols and diols by hydrogenation of carboxylic acids and esters over Ru–Sn–Al2O3 catalysts. *Applied Catalysis A: General* **1999,** *189* (2), 243-250.
8. He, D.-H.; Wakasa, N.; Fuchikami, T., Hydrogenation of carboxylic acids using bimetallic catalysts consisting of group 8 to 10, and group 6 or 7 metals. *Tetrahedron Letters* **1995,** *36* (7), 1059-1062.
9. Rozmysłowicz, B.; Kirilin, A.; Aho, A.; Manyar, H.; Hardacre, C.; Wärnå, J.; Salmi, T.; Murzin, D. Y., Selective hydrogenation of fatty acids to alcohols over highly dispersed ReOx/TiO2 catalyst. *Journal of Catalysis* **2015,** *328*, 197-207.
10. Manyar, H. G.; Paun, C.; Pilus, R.; Rooney, D. W.; Thompson, J. M.; Hardacre, C., Highly selective and efficient hydrogenation of carboxylic acids to alcohols using titania supported Pt catalysts. *Chemical Communications* **2010,** *46* (34), 6279-6281.

11. Kandel, K.; Chaudhary, U.; Nelson, N. C.; Slowing, I. I., Synergistic Interaction between Oxides of Copper and Iron for Production of Fatty Alcohols from Fatty Acids. *ACS Catalysis* **2015,** *5* (11), 6719-6723.
12. Si, R.; Raitano, J.; Yi, N.; Zhang, L.; Chan, S.-W.; Flytzani-Stephanopoulos, M., Structure sensitivity of the low-temperature water-gas shift reaction on Cu–CeO2 catalysts. *Catalysis Today* **2012,** *180* (1), 68-80.
13. Tang, X.; Zhang, B.; Li, Y.; Xu, Y.; Xin, Q.; Shen, W., CuO/CeO2 catalysts: Redox features and catalytic behaviors. *Applied Catalysis A: General* **2005,** *288* (1–2), 116-125.
14. Tabakova, T.; Boccuzzi, F.; Manzoli, M.; Sobczak, J. W.; Idakiev, V.; Andreeva, D., A comparative study of nanosized IB/ceria catalysts for low-temperature water-gas shift reaction. *Applied Catalysis A: General* **2006,** *298* (0), 127-143.
15. Sakata, Y.; Ponec, V., Reduction of benzoic acid on CeO2 and, the effect of additives. *Applied Catalysis A: General* **1998,** *166* (1), 173-184.
16. Yokoyama, T.; Yamagata, N., Hydrogenation of carboxylic acids to the corresponding aldehydes. *Applied Catalysis A: General* **2001,** *221* (1–2), 227-239.
17. Cheng, D.-G.; Chong, M.; Chen, F.; Zhan, X., XPS Characterization of CeO2 Catalyst for Hydrogenation of Benzoic Acid to Benzaldehyde. *Catalysis Letters* **2008,** *120* (1-2), 82-85.
18. Vivier, L.; Duprez, D., Ceria-Based Solid Catalysts for Organic Chemistry. *ChemSusChem* **2010,** *3* (6), 654-678.
19. Nelson, N. C.; Manzano, J. S.; Sadow, A. D.; Overbury, S. H.; Slowing, I. I., Selective Hydrogenation of Phenol Catalyzed by Palladium on High-Surface-Area Ceria at Room Temperature and Ambient Pressure. *ACS Catalysis* **2015,** *5* (4), 2051-2061.
20. Cao, J.-L.; Wang, Y.; Zhang, T.-Y.; Wu, S.-H.; Yuan, Z.-Y., Preparation, characterization and catalytic behavior of nanostructured mesoporous CuO/Ce0.8Zr0.2O2 catalysts for low-temperature CO oxidation. *Applied Catalysis B: Environmental* **2008,** *78* (1–2), 120-128.
21. Bera, P.; Priolkar, K. R.; Sarode, P. R.; Hegde, M. S.; Emura, S.; Kumashiro, R.; Lalla, N. P., Structural Investigation of Combustion Synthesized Cu/CeO2 Catalysts by EXAFS and Other Physical Techniques: Formation of a Ce1-xCuxO2-δ Solid Solution. *Chemistry of Materials* **2002,** *14* (8), 3591-3601.
22. Luo, M.-F.; Zhong, Y.-J.; Yuan, X.-X.; Zheng, X.-M., TPR and TPD studies of CuOCeO2 catalysts for low temperature CO oxidation. *Applied Catalysis A: General* **1997,** *162* (1–2), 121-131.
23. Xiaoyuan, J.; Guanglie, L.; Renxian, Z.; Jianxin, M.; Yu, C.; Xiaoming, Z., Studies of pore structure, temperature-programmed reduction performance, and micro-structure of CuO/CeO2 catalysts. *Applied Surface Science* **2001,** *173* (3–4), 208-220.
24. Ciston, J.; Si, R.; Rodriguez, J. A.; Hanson, J. C.; Martínez-Arias, A.; Fernandez-García, M.; Zhu, Y., Morphological and Structural Changes during the Reduction and Reoxidation of CuO/CeO2 and Ce1–xCuxO2 Nanocatalysts: In Situ Studies with Environmental TEM, XRD, and XAS. *The Journal of Physical Chemistry C* **2011,** *115* (28), 13851-13859.
25. Bernal, S.; Calvino, J. J.; Cifredo, G. A.; Rodriguez-Izquierdo, J. M., Comments on "Redox Processes on Pure Ceria and Rh/CeO2 Catalyst Monitored by X-ray Absorption (Fast Acquisition Mode). *The Journal of Physical Chemistry* **1995,** *99* (30), 11794-11796.

26. Wang, X.; Rodriguez, J. A.; Hanson, J. C.; Gamarra, D.; Martínez-Arias, A.; Fernández-García, M., In Situ Studies of the Active Sites for the Water Gas Shift Reaction over Cu−CeO2 Catalysts: Complex Interaction between Metallic Copper and Oxygen Vacancies of Ceria. *The Journal of Physical Chemistry B* **2006,** *110* (1), 428-434.

CHAPTER 3
SYNTHESIS OF NITROGEN CONTAINING MESOPOROUS CARBON

In this report we introduce aspartic acid as a carbon precursor to synthesize nitrogen containing mesoporous carbon materials by the hard template method. Thus obtained carbons have high nitrogen content (13.10 wt % at carbonization temperature 500 °C) and were tested as catalysts and supports for Fe catalyst in aldol condensation and hydrogenation reaction respectively.

Introduction

The synthesis of porous materials attracts intensive attention for its applications in diverse areas such as heterogeneous catalysis, adsorption, gas sensing, energy storage and electrochemistry.[1,2,3,4,5] Significant advances have been made to control the structural, compositional and morphological properties of these materials.[6] Porous materials are classified into three different groups based on their pore sizes: below 2 nm are microporous, between 2 nm and 50 nm are mesoporous and above 50 nm are macroporous.[7] Microporous materials like zeolites have been extensively studied for diverse applications.[8,9] Moreover, the applications of zeolites are limited to small molecules in the gas phase because of their pore size. This has drawn researchers' attention towards developing mesoporous materials. Like Zeolites, mesoporous silicas have high surface areas and pore volumes but pore diameters between 2 nm and 50 nm. Controlled modification of the pore structure and the surface chemistry have made mesoporous silica useful in applications like catalysis, adsorption, etc.[10,11,12] However, silica materials are not hydrothermally stable. In this regard, mesoporous carbons present an important alternative because of their higher stability to aqueous media.

The application of carbon in various fields like catalysis and separations can benefit from controlling their chemical composition.[13,14] Carbons that are especially doped with nitrogen have gained much attention for their unique properties.[15] They have been reported to be useful in applications like catalysis, CO_2 capture, metal adsorption, etc.[16,17,18] The post synthesis treatment of mesoporous carbon can be done by treatment with ammonia or acetonitrile to incorporate nitrogen functionalities into the carbon framework.[19,20,21] Such post modification strategy has some flaws associated with damage to the carbon surface or pore structure.[22,23] N-doped carbons can also be prepared using nano-casting strategy with sacrificial templates.[24,25] Choice of carbon precursor is important in this method as it is the source of nitrogen as well. Recently, ionic liquids have been reported as attractive alternatives to synthesize N-doped carbon.[26,27] Because they are non-volatile and decompose below their boiling point, these liquids are known to undergo poly-condensation and subsequent aromatization resulting in graphitic structures under thermal treatment. However, ionic liquids are very expensive and they have quite low yields in carbonization. In this regard, amino acids such as aspartic acid are attractive carbon precursors owing to their capacity to polymerize at low temperatures (200-270 ^{o}C) and their bifunctional structure.[28,29] In addition, amino acids are abundant in biomass which makes these carbon precursors bio-renewable.

In this report, we introduce aspartic acid as a precursor for developing nitrogen functionalized mesoporous carbon using the hard template method.

Experimental Section

Reagents

Pluronic P104 was provided by BASF. Tetramethyl orthosilicate (TMOS), and L-aspartic acid were purchased from Sigma-Aldrich. Ethanol was purchased from Decon Laboratories; sulfuric acid and sodium hydroxide were purchased from Fisher Scientific. All the reagents were used without further purification.

Synthesis of Mesoporous Silica Nanoparticles (MSN)

MSN was prepared using a nonionic block copolymer Pluronic P104 surfactant using a previously reported procedure.[30] In a typical synthesis, P104 (7.0 g, 1.19 mmol) was added to HCl (109 ml, 4 M, 0.436 mmol) and de-ionized H_2O (164 g, 9.11 mol). After stirring for 1 h at 52 °C, tetramethylorthosilicate (TMOS, 10.64 g, 70.1 mmol) was added and stirred for an additional 24 h. The resulting mixture was further aged for 24 h at 150 °C in a Teflon-lined autoclave. Upon cooling to room temperature, the white solid was collected by filtration, washed with copious amounts of water and methanol, and dried in a lypholizer. Finally the P-104 template was removed by calcining the MSN material at a ramp rate of 2.0 °C min^{-1}, and holding the temperature at 550 °C for 6 h

Synthesis of Mesoporous Carbon

For the synthesis of mesoporous carbon, aspartic acid solution was prepared first by dissolving aspartic acid (1.43 g, 10.7 mmol) in 80 ml H_2O under 80 ^oC heat treatment and vigorous stirring for 5-7 minutes. MSN (1.0 g) was then dispersed in the aspartic acid solution and concentrated H_2SO_4 (87.0 μL, 1.63 mmol) was added to it. The mixture was dried in an oven at 100 °C for 6 h followed by heating under air at 270 °C for 6 h. After

letting the solid cool to room temperature, 0.775 g (5.82 mmol) of aspartic acid (dissolved in 80 ml H_2O) and H_2SO_4 (87.0 μL, 1.63 mmol) was added to the resulting composite which was further dried at 100 °C for 6 h followed by additional heating at 270 °C for another 6 h. The as prepared material was then carbonized at different temperatures (500 °C, 700 °C and 900 °C) under nitrogen at heating rate of 5 °C min^{-1}. Finally the silica template was removed by refluxing the carbonized materials in a 2M solution of NaOH in ethanol-water (v/v=1:1), washed several times with water via filtration until the pH of the filtrate is neutral. The final materials were further dried in lypholizer under vacuum. Based on the carbonization temperature: 500 °C, 700 °C, 900 °C, the final materials were categorized as C-500, C-700 and C-900.

Characterization

Surface analysis of the carbon materials were measured by nitrogen sorption isotherm in Micromeritics Tristar analyzer. The surface areas were calculated by the Brunauer−Emmett−Teller (BET) method, and the pore size distribution was calculated by the Barret-Joyner-Halenda (BJH) method. Small angle powder X-ray diffraction patterns were obtained using a Bruker AXS D8 Discover powder diffractometer at 40 kV, 40 mA for Cu Kα, (λ = 1.5406 Å) in a continuous fast mode using a Linxeye Xe detector. Fourier transform infrared (FT-IR) spectra were recorded on Brukers' Vertex 80 spectrophotometer. The samples were dried at 110 ^oC under vacuum over 12 h before FT-IR analysis. ICP-OES was used to measure Si content in the carbons. To prepare samples for ICP analysis, carbon samples (4 mg) were treated with NaOH solution (10 ml, 2M) for over 48 h. The solids were then separated by centrifugation and the supernatant (2 ml) was neutralized with hydrochloric acid solution (2 ml, 2 M). CHNS elemental analysis was done on dry carbon samples by

triplicates on Perkin Elmer 2100 Series II CNHS analyzer using acetanilide (ACE) as calibration standard at combustion temperature of 925 ^{o}C. Carbon samples were dried under vacuum at 110 ^{o}C overnight before CHNS analysis. For acid base titrations each carbon was dispersed in HCl and NaOH solution for over 24 h in separate experiments and the solid was separated by centrifugation. Then the aliquot was back titrated using NaOH and HCl for determining the number of basic and acidic sites respectively. XPS analysis was done using PHI 5500 multitechnique system with a standard Al X-Ray source.

Results and Discussions

Structural properties of the Mesoporous Carbon

The N_2 adsorption-desorption isotherms of all the carbons are shown in Figure 16b. Regardless of carbonization temperature all the materials showed Type IV isotherms. The pore size distribution of all the carbon materials in the range of 3 to 6 nm indicated their mesoporous nature (Figure 16a). A small angle X-ray diffraction of MSN used as a template showed a well ordered 2D hexagonal pattern. Similarly the diffraction peaks of C-500, C-700 and C-900 carbons indicated their good degree of pore ordering (Figure 16c).

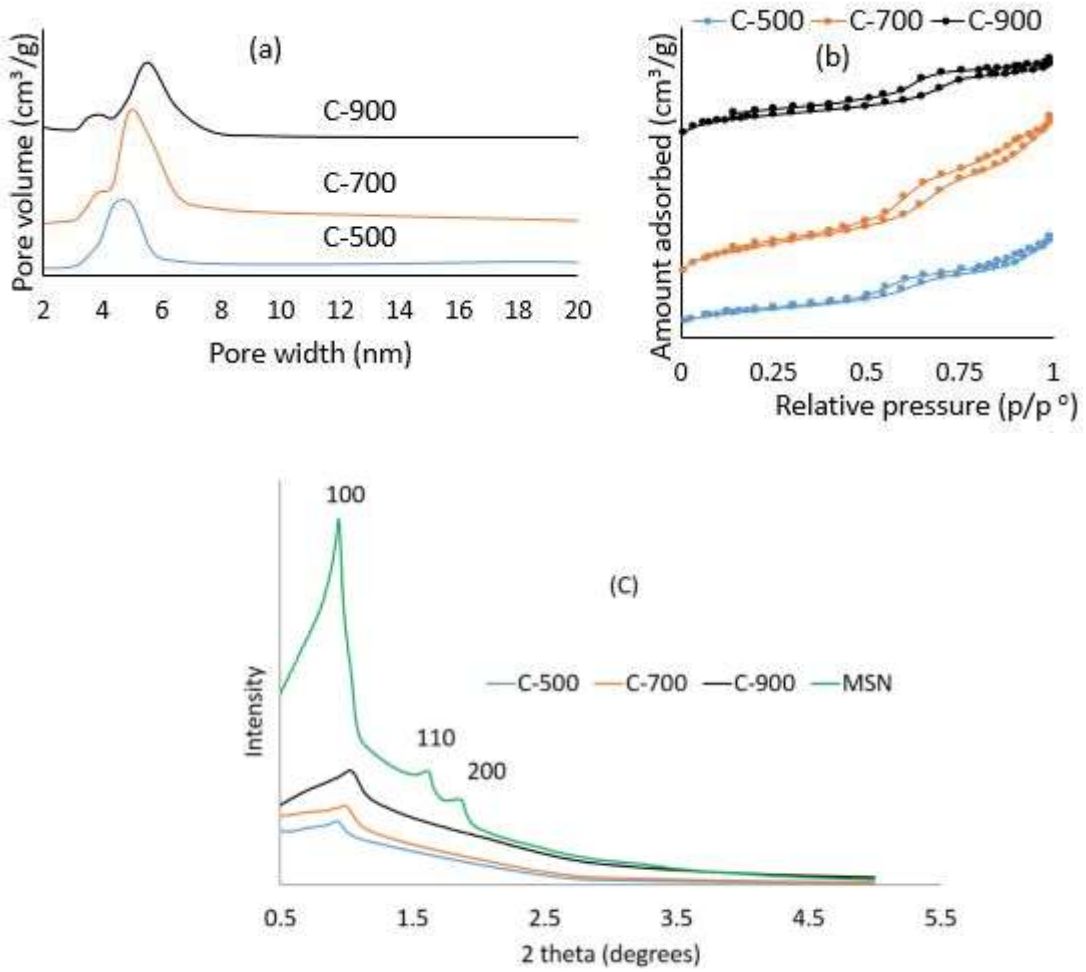

Figure 16 a) Pore size distribution of C-500, C-700 and C-900 b) their linear isotherm and c) their low angle X-ray diffraction patterns including MSN template

The textural properties of the carbons are shown in Table 4. The results indicate the effect of carbonization temperature on surface area, pore volume and pore width. Literatures have shown that an appropriate carbonization temperature is needed to control textural properties in the carbon.[31] A bimodal pore size distribution is seen in both C-700 and C-900. Reports have attributed the small pore and larger pore to pores forming from silica pore wall and voids caused by partial unoccupied silica template respectively.[32] A control (C-500**) was also prepared without using a MSN template and its textural properties were studied using BET experiment. The surface area and pore volume of this material are 0.781 m^2/g and

0.0161 m^2/g respectively which is insignificant compared to carbons prepared using template. This suggests that silica template was indispensable for developing mesoporous carbon using aspartic acid precursor. The complete removal of silica template is important to ensure the textural properties actually correspond to the carbon and not to residual MSN template. ICP-OES results showed less than 0.2 wt % of silicon was present in all of the carbons. This confirms the mesoporous carbon prepared were almost silica free.

Table 4 Surface properties of the materials

Material	Surface area (m^2/g)	Pore volume (cm^3/g)	BJH Pore Width (nm)
C-900	294	0.229	4.35, 5.56
C-700	402	0.414	4.32, 4.94
C-500	126	0.183	4.68
C-500**	0.781	0.0162	--
MSN template	461	1.23	7.1

C-500** is the control carbon sample prepared in a similar manner at carbonization temperature 500 °C without MSN template

Chemical properties of the Mesoporous Carbon

To study the elemental composition of the carbons we performed CNH elemental analysis (Table 5). C-500 contains 13.1 wt % nitrogen while the amount of nitrogen goes down to 1.55 wt % with the increase in temperature to 900 ^oC as expected, likely lost as N_2. Similarly, the amount of hydrogen in carbon goes down with the increase in carbonization temperature. These results show the importance of carbonization temperature in retaining the amount of nitrogen in the materials. Also, with the increase in carbonization temperature from 500 °C to 700 °C the carbon content increases from 56.27 wt% to 75.69 wt % as expected. But surprisingly, it remains same for C-700 and C-900. Further, the amount of oxygen in each carbons were also calculated using 100 – (% C + % H + %N) and listed in

Table 5 (column 5). It is unexpected that C-900 shows 21.86 % O which is higher than that of C-700 (16.42 % O). This may be due to adsorption of atmospheric water on the C-900. These results may suggest that both nitrogen and oxygen can be partially retained in the carbon.

Titration was used to study the acidic and basic properties of these carbons. Table 5 (columns 5 and 6) shows both acidic and basic properties of the carbons. Interestingly, the amount of basic sites determined by titration did not follow similar decreasing trend with the elemental analysis results. CNH results showed the decrease in nitrogen amount with the increase in carbonization temperature. But the basic sites as determined by titration in C-700 and C-900 are still higher than that of C-500 even though C-500 has higher weight % of nitrogen. There may be many possible reasons for this discrepancies: C-500 material may have nitrogen embedded into the framework which are not easily accessible or the higher carbonization temperature could be transforming the nitrogen groups in the material into different types of N-heterocycles as explained in the next section.

Table 5 CNH elemental analysis

Material	% C	% H	% N	% O (by difference)	Basic sites (mmol/g)[a]	Acidic sites (mmol/g)[a]
C-900	75.88	0.71	1.55	28.15	0.410	0.576
C-700	75.69	1.11	6.78	16.42	0.818	0.383
C-500	56.27	2.48	13.10	21.86	0.630	0.345

[a] acidic and basic sites were determined by titration

To further identify the functional groups we performed FT-IR studies on the carbon as shown in Figure 17. The peaks at 1517 and 1464 cm^{-1} indicate C=C bond of aromatics. These peaks were well resolved and intense for C-700 and C-900 compared to C-500, which

might suggest at higher carbonization temperature, carbons are becoming more aromatic. A stretch at 3440 cm^{-1} might indicate the presence of N-H or O-H stretching vibrations. The band around 1609 cm^{-1} is attributed to aromatic C=N stretching while the bands at 1262 cm^{-1} and 1376 cm^{-1} are attributed to stretching vibrations of aromatic bonds CN in condensed CN-heterocycles.[33] Hence the FT-IR analysis suggests the existence of N-H and C-N species in the resultant mesoporous carbons.

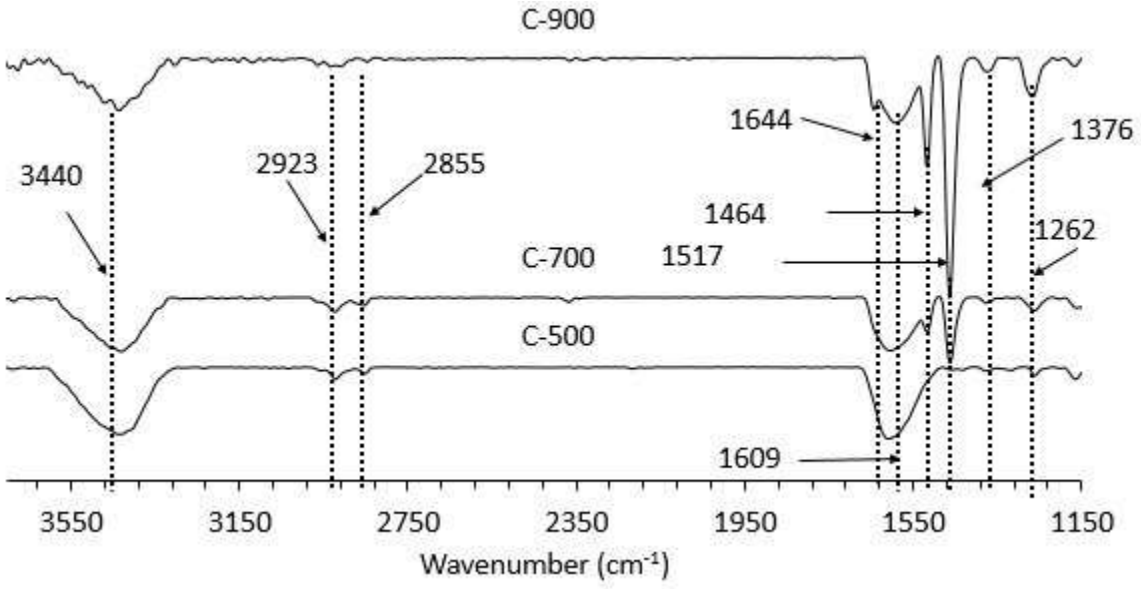

Figure 17 FT-IR of C-500, C-700 and C-900

We further used XPS to study the nature of nitrogen and oxygen functionalities in the carbon. Figure 18 shows the XPS spectra of C-500. N1s and O1s spectra are fitted to get detailed chemical bonding information of N and O elements. N1s deconvolution shows there are 3 types of nitrogen in C-500: pyridinic- N (398.5 eV), pyrrolic- N (399.5 eV) and quaternary- N (402 eV).[34] Pyridinic- N generally refers to N atoms at the edge of graphene planes each of which is bonded to two carbon atoms and donates one p electron to aromatic

pi system, pyrrolic- N refers to N atoms bonded to two carbon atoms and contribute two p electrons to the pi system and quaternary-N refers to substitution nitrogen or graphitic nitrogen in which N atoms replace carbon atoms within graphene plane.[34] The existence of pyridinic and pyrrolic nitrogen as shown by XPS results supports the presence C=N bond as shown by FT-IR. The relative amount of these three types of nitrogen were also calculated based on the area of deconvolution as shown in Table 6. Our results show the presence of 37.8 % of pyridinic nitrogen, 47.1 % of pyrrolic nitrogen and 15.1 % of quaternary nitrogen.

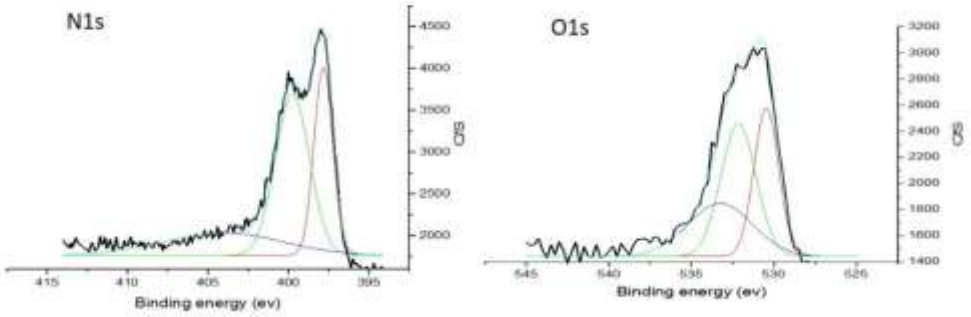

Figure 18 XPS of C-500

Table 6 Relative amount of nitrogen species in C-500 by XPS

Binding energy (eV)	Nitrogen types	Relative amount
398.5	pyridinic	37.8
399.5	pyrrolic	47.1
401-405	quaternary	15.1

Similarly, O1s deconvolution shows three types of oxygen species present in C-500 as listed in Table 7.[35] The presence of OH species as suggested by XPS analysis supports the existence of OH stretch as shown by FT-IR in C-500. Pyridinic- N are known to be more basic than pyrrolic- N and quaternary- N. Different literatures have reported that pyridinic- N and pyrrolic- N predominantly form at lower temperature (~ 500 ^{o}C) which may transform

into more thermally stable quaternary N at higher temperature (> 750 ºC).[36,37] If this holds true in our case then we would expect C-700 and C-900 would exhibit different types of nitrogen species which would account for the variation in basicity with temperature.

Table 7 Relative amount of oxygen species in C-500 by XPS

Binding energy (eV)	Oxygen types	Relative amount
530.9	C=O	41.1
532.3	C-OH	35.3
533.7	C-O	23.6

Aldol Condensation

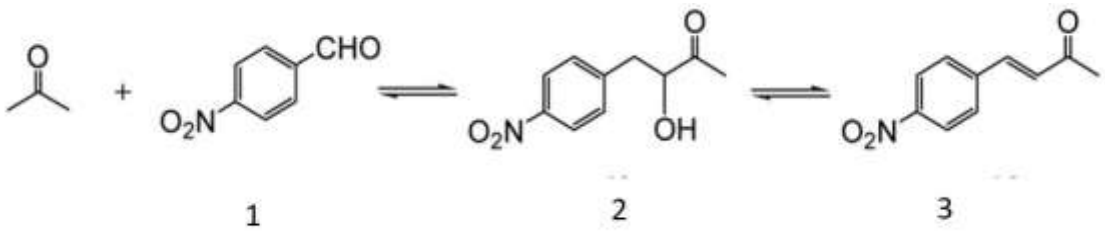

Scheme 1: Aldol condensation (Conditions: 10 mg 4-nitrobenzaldehyde, 5 mol % accessible basic groups, 60 ºC, Solvent (5 ml total volume), 20 h)

We investigated the nitrogen containing mesoporous carbon as a catalyst for the aldol condensation of acetone with 4-nitrobenzaldehyde at 60 ºC for 20 h in various solvents (5 ml total volume): acetone, acetone: DMSO = 4:1 volume ratio and acetone: water = 4:1 volume ratio using 5 mol % accessible basic sites. The accessible basic sites are based on titration results for each carbon. None of the materials showed any activity using neat acetone or acetone: DMSO mixtures as solvents. Switching the solvent to acetone: water, all carbons were active for the condensation reaction (Table 8). Studies of the effect of water in the aldol condensation have been previously reported elsewhere.[38,39] They have demonstrated the role of water in the regeneration of active basic group (amines) at the expense of the inactive iminium form. This kind of observation is unlikely in our case as we don't expect to have

amines in our carbons based on our investigations. Moreover, the carbons showed differences in % yield of "3" as shown in Table 8. Such differences in % yield of 3 may be due to the presence of different basic species in these carbons. Further characterization of the materials need to be done to draw a definitive conclusion.

Table 8 Conversion of 4-nitrobenzaldehyde

Catalysts	Solvent	% Yield of 3	TON
C-500	Acetone/water = 4:1	69	13.8
C-700	Acetone/water = 4:1	53	10.6
C-900	Acetone/water = 4:1	45	9.0

Hydrogenation of Nitrobenzene

We used our carbon as a support for iron precursor to investigate the hydrogenation of nitrobenzene into aniline. C-500 was supported with iron (III) acetate followed by pyrolysis under nitrogen at 300 ^{o}C held for 2 h and used as catalyst in the hydrogenation of nitrobenzene.

Scheme 2: Hydrogenation of nitrobenzene (Conditions: 1 mmol nitrobenzene, 0.3 mol % Fe, 10 bar H_2, H_2O: THF =1:1 (10 ml total volume), 120 ^{o}C, 3h)

The 46 ± 11 % yield of aniline was obtained using only 0.3 mol % Fe as catalyst. The activity of this catalyst is higher than the literature reported shown below:

Table 9 Hydrogenation of nitrobenzene into aniline

Catalysts	TOF	Conditions	References
Fe_xO_y-carbon	39	120 ^{o}C, 10 bar H_2, 3 h	This work
Fe_2O_3-carbon	1.5	120 ^{o}C, 50 bar H_2, 15 h	17

The higher hydrogenation activity showed by our catalyst may be ascribed to the presence of oxygen functionality in our catalyst which is lacking in the Fe_2O_3-carbon catalyst reported by Jagadeesh et al. Wang and collaborators have reported the promotion of H – spillover in carbon due to presence of oxygen functionality like hydroxyl and carboxyl in the carbon.[40]

Conclusions

In this study we successfully developed nitrogen containing mesoporous carbons using aspartic acid via hard template method. The as synthesized carbon materials were active for aldol condensation of 4-nitrobenzaldehyde with acetone. Similarly, C-500 was used as a support to load iron catalyst that was active in the hydrogenation of nitrobenzene to aniline. Further investigation on the characterization of the catalysts will provide insight on the catalytic behavior of these carbons.

References

1. Zhao, M.; Ou, S.; Wu, C.-D., Porous Metal–Organic Frameworks for Heterogeneous Biomimetic Catalysis. *Accounts of Chemical Research* **2014,** *47* (4), 1199-1207.
2. Akhtar, F.; Andersson, L.; Ogunwumi, S.; Hedin, N.; Bergström, L., Structuring adsorbents and catalysts by processing of porous powders. *Journal of the European Ceramic Society* **2014,** *34* (7), 1643-1666.
3. Ma, J.; Teo, J.; Mei, L.; Zhong, Z.; Li, Q.; Wang, T.; Duan, X.; Lian, J.; Zheng, W., Porous platelike hematite mesocrystals: synthesis, catalytic and gas-sensing applications. *Journal of Materials Chemistry* **2012,** *22* (23), 11694-11700.
4. Vix-Guterl, C.; Frackowiak, E.; Jurewicz, K.; Friebe, M.; Parmentier, J.; Béguin, F., Electrochemical energy storage in ordered porous carbon materials. *Carbon* **2005,** *43* (6), 1293-1302.
5. Zhang, C.; Hatzell, K. B.; Boota, M.; Dyatkin, B.; Beidaghi, M.; Long, D.; Qiao, W.; Kumbur, E. C.; Gogotsi, Y., Highly porous carbon spheres for electrochemical capacitors and capacitive flowable suspension electrodes. *Carbon* **2014,** *77*, 155-164.
6. Mingle, J. O.; Smith, J. M., Effectiveness factors for porous catalysts. *AIChE Journal* **1961,** *7* (2), 243-249.
7. Sing, K. S. W.; Everett, D. H.; Haul, R. A. W.; Moscou, L.; Pierotti, R. A.; Rouquerol, J.; Siemieniewska, T., Reporting physisorption data for gas/solid systems with special reference to the determination of surface area and porosity. *Pure Appl. Chem.* **1985,** *57* (4), 603-619.
8. *Zeolites in Industrial Separation and Catalysis*. Wiley-VCH Verlag GmbH & Co. KGaA: 2010.
9. Front Matter. In *Modern Drying Technology*, Wiley-VCH Verlag GmbH & Co. KGaA: 2011; pp I-XXXV.
10. Kandel, K.; Chaudhary, U.; Nelson, N. C.; Slowing, I. I., Synergistic Interaction between Oxides of Copper and Iron for Production of Fatty Alcohols from Fatty Acids. *ACS Catalysis* **2015,** *5* (11), 6719-6723.
11. Kandel, K.; Frederickson, C.; Smith, E. A.; Lee, Y.-J.; Slowing, I. I., Bifunctional Adsorbent-Catalytic Nanoparticles for the Refining of Renewable Feedstocks. *ACS Catalysis* **2013,** *3* (12), 2750-2758.
12. Valenstein, J. S.; Kandel, K.; Melcher, F.; Slowing, I. I.; Lin, V. S. Y.; Trewyn, B. G., Functional Mesoporous Silica Nanoparticles for the Selective Sequestration of Free Fatty Acids from Microalgal Oil. *ACS Applied Materials & Interfaces* **2012,** *4* (2), 1003-1009.
13. Yang, Y.; Zhang, J.; Zhuang, J.; Wang, X., Synthesis of nitrogen-doped carbon nanostructures from polyurethane sponge for bioimaging and catalysis. *Nanoscale* **2015,** *7* (29), 12284-12290.
14. Chandra, V.; Yu, S. U.; Kim, S. H.; Yoon, Y. S.; Kim, D. Y.; Kwon, A. H.; Meyyappan, M.; Kim, K. S., Highly selective CO_2 capture on N-doped carbon produced by chemical activation of polypyrrole functionalized graphene sheets. *Chemical Communications* **2012,** *48* (5), 735-737.
15. Kinoshita, K., *Carbon: Electrochemical and Physicochemical Properties*. Wiley: Newyork, 1998.

16. Li, D.; Chen, Y.; Zheng, M.; Zhao, H.; Zhao, Y.; Sun, Z., Hierarchically Structured Porous Nitrogen-Doped Carbon for Highly Selective CO2 Capture. *ACS Sustainable Chemistry & Engineering* **2016,** *4* (1), 298-304.
17. Jagadeesh, R. V.; Surkus, A. E.; Junge, H.; Pohl, M. M.; Radnik, J.; Rabeah, J.; Huan, H.; Schunemann, V.; Bruckner, A.; Beller, M., Nanoscale Fe_2O_3-based catalysts for selective hydrogenation of nitroarenes to anilines. *Science* **2013,** *342* (6162), 1073-1076.
18. Shin, K.-Y.; Hong, J.-Y.; Jang, J., Heavy metal ion adsorption behavior in nitrogen-doped magnetic carbon nanoparticles: Isotherms and kinetic study. *Journal of Hazardous Materials* **2011,** *190* (1–3), 36-44.
19. Hou, Z.; Terakura, K., Effect of Nitrogen Doping on the Migration of the Carbon Adatom and Monovacancy in Graphene. *The Journal of Physical Chemistry C* **2015,** *119* (9), 4922-4933.
20. Xia, Y.; Mokaya, R., Generalized and Facile Synthesis Approach to N-Doped Highly Graphitic Mesoporous Carbon Materials. *Chemistry of Materials* **2005,** *17* (6), 1553-1560.
21. Wang, X.; Lee, J. S.; Zhu, Q.; Liu, J.; Wang, Y.; Dai, S., Ammonia-Treated Ordered Mesoporous Carbons as Catalytic Materials for Oxygen Reduction Reaction. *Chemistry of Materials* **2010,** *22* (7), 2178-2180.
22. Bahr, J. L.; Tour, J. M., Covalent chemistry of single-wall carbon nanotubes. *Journal of Materials Chemistry* **2002,** *12* (7), 1952-1958.
23. Martin-Hopkins, M. B.; Gilpin, R. K.; Jaroniec, M., Studies of the Surface Heterogeneity of Chemically Modified Porous Carbons by Gas-Solid Chromatography. *Journal of Chromatographic Science* **1991,** *29* (4), 147-152.
24. Lei, Z.; Bai, D.; Zhao, X. S., Improving the electrocapacitive properties of mesoporous CMK-5 carbon with carbon nanotubes and nitrogen doping. *Microporous and Mesoporous Materials* **2012,** *147* (1), 86-93.
25. Yang, C.-M.; Weidenthaler, C.; Spliethoff, B.; Mayanna, M.; Schüth, F., Facile Template Synthesis of Ordered Mesoporous Carbon with Polypyrrole as Carbon Precursor. *Chemistry of Materials* **2005,** *17* (2), 355-358.
26. Paraknowitsch, J. P.; Thomas, A.; Antonietti, M., A detailed view on the polycondensation of ionic liquid monomers towards nitrogen doped carbon materials. *Journal of Materials Chemistry* **2010,** *20* (32), 6746-6758; Lim, K. H.; Kim, H., Nitrogen-doped carbon catalysts derived from ionic liquids in the presence of transition metals for the oxygen reduction reaction. *Applied Catalysis B: Environmental* **2014,** *158–159*, 355-360.
27. Zhang, S.; Miran, M. S.; Ikoma, A.; Dokko, K.; Watanabe, M., Protic Ionic Liquids and Salts as Versatile Carbon Precursors. *Journal of the American Chemical Society* **2014,** *136* (5), 1690-1693.
28. Nakato, T.; Kusuno, A.; Kakuchi, T., Synthesis of poly(succinimide) by bulk polycondensation of L-aspartic acid with an acid catalyst. *Journal of Polymer Science Part A: Polymer Chemistry* **2000,** *38* (1), 117-122.
29. Wang, Y.; Hou, Y.; Zhang, J.; Ruan, G., Kinetics of dehydration–polymerization of aspartic acid and synthesis of polyaspartate catalyzed by potassium bisulfate. *Polymer International* **2004,** *53* (2), 156-162.
30. Kim, T.-W.; Slowing, I. I.; Chung, P.-W.; Lin, V. S.-Y., Ordered Mesoporous Polymer−Silica Hybrid Nanoparticles as Vehicles for the Intracellular Controlled Release of Macromolecules. *ACS Nano* **2011,** *5* (1), 360-366.

31. Katesa, J.; Junpiromand, S.; Tangsathitkulchai, C., Effect of carbonization temperature on properties of char and activated carbon from coconut shell. *Suranaree journal of science and technology* **2013,** *20* (4), 269.
32. Lu, A. H.; Schmidt, W.; Spliethoff, B.; Schüth, F., Synthesis of Ordered Mesoporous Carbon with Bimodal Pore System and High Pore Volume. *Advanced Materials* **2003,** *15* (19), 1602-1606.
33. Kharlamov, A.; Bondarenko, M.; Kharlamova, G.; Gubareni, N.; Fomenko, V., A new method of synthesis carbon with onion-like structure with (10-13 %) content of nitrogen from pyridine. *Universal Journal of Materials Science* **2013,** *1* (2), 78-86.
34. Shao, Y.; Zhang, S.; Engelhard, M. H.; Li, G.; Shao, G.; Wang, Y.; Liu, J.; Aksay, I. A.; Lin, Y., Nitrogen-doped graphene and its electrochemical applications. *Journal of Materials Chemistry* **2010,** *20* (35), 7491-7496.
35. Lakshminarayanan, P. V.; Toghiani, H.; Pittman Jr, C. U., Nitric acid oxidation of vapor grown carbon nanofibers. *Carbon* **2004,** *42* (12–13), 2433-2442.
36. van Dommele, S.; Romero-Izquirdo, A.; Brydson, R.; de Jong, K. P.; Bitter, J. H., Tuning nitrogen functionalities in catalytically grown nitrogen-containing carbon nanotubes. *Carbon* **2008,** *46* (1), 138-148.
37. Choi, H. C.; Bae, S. Y.; Jang, W.-S.; Park, J.; Song, H. J.; Shin, H.-J.; Jung, H.; Ahn, J.-P., Release of N2 from the Carbon Nanotubes via High-Temperature Annealing. *The Journal of Physical Chemistry B* **2005,** *109* (5), 1683-1688.
38. Zotova, N.; Franzke, A.; Armstrong, A.; Blackmond, D. G., Clarification of the Role of Water in Proline-Mediated Aldol Reactions. *Journal of the American Chemical Society* **2007,** *129* (49), 15100-15101.
39. Kandel, K.; Althaus, S. M.; Peeraphatdit, C.; Kobayashi, T.; Trewyn, B. G.; Pruski, M.; Slowing, I. I., Solvent-Induced Reversal of Activities between Two Closely Related Heterogeneous Catalysts in the Aldol Reaction. *ACS Catalysis* **2013,** *3* (2), 265-271.
40. Wang, L.; Yang, F. H.; Yang, R. T.; Miller, M. A., Effect of Surface Oxygen Groups in Carbons on Hydrogen Storage by Spillover. *Industrial & Engineering Chemistry Research* **2009,** *48* (6), 2920-2926.

CHAPTER 4
GENERAL CONCLUSIONS

The importance of developing high surface area nanomaterials for catalysis has been recognized for decades. The projects described in this thesis show the development of two such nanomaterials, characterization and their potential application in catalysis.

Ceria is an interesting material in the context of catalysis. Most of the catalytic works based on ceria materials are focused on oxidation reactions. In Chapter 2, we have discussed the potential application of copper oxide supported on ceria for selective hydrogenation of fatty acids. Our results indicate that these catalysts are active hydrogenation catalysts at low pressure (5 bar H_2) that give alcohol or alkanes as products depending on the amount of copper loaded on the ceria support. A Cu/Ce mole ratio of 0.05 in the composite catalyst showed high selective reduction of acids to alcohols. As Cu/Ce mol ratio is increased, the alkanes selectivity increased at the expense of alcohol selectivity. We think generation of enough activated H_2 in the high copper loaded catalysts may lead to the subsequent reduction of alcohols into alkanes. Studies of the dispersion of copper on the support may provide further insights on the catalytic behavior of these composite catalysts. We have shown that copper oxide and ceria act synergistically in the conversion of fatty acids into fatty alcohols. We believe metallic copper and oxygen vacancies formed under reaction conditions act as active sites for this system. Further, characterizations using spectroscopic techniques may be useful in understanding the mechanism of this system.

In chapter 3, we have discussed the development of nitrogen containing mesoporous carbons using aspartic acid as organic precursor via hard template method. Based on the textural studies by N_2 physisorption, we learned the carbons exhibit high surface area and

mesoporosity. Our XPS results indicate the presence of three types of nitrogen: pyridinic, pyrrolic and quaternary in the carbons carbonized at 500 ^{o}C. Further, our FT-IR results suggest the presence of pyridinic-N in all the carbons carbonized at different temperatures. We believe the pyridinic-N, which is basic is responsible for the catalytic activity of the carbon towards the aldol condensation. Interestingly, we observed differences in catalytic activities using carbons prepared at different temperatures for the aldol condensation. Structural characterizations may provide further insights on the catalytic behavior of these basic catalysts. The carbons were also used as supports for iron catalysts in the hydrogenation of nitrobenzene to aniline. These results open a path for investigating amino acids as precursors for developing nitrogen containing high surface area catalysts.

APPENDIX A
GC-MS RAW DATA OF INVESTIGATIONS ON STEARIC ACID HYDROGENATION

Adsorption test of stearic acid and octadecanol with ceria

Stearic acid adsorption test: 10 ml (10 mM) of stearic acid was mixed with 10 mg of ceria in a vial and left for stirring for 3h at room temperature. The solid was separated by centrifugation and 1 ml of aliquot was reacted with 0.25 ml sylon BFT for acid derivatization. Finally 60 µL of derivatized aliquot was mixed with 920 µL of hexane and 1-methylnonadecanoate (20 µL, 8 mM) as internal standard (I.S.) in gc vial and analyzed by GC-MS.

Octadecanol adsorption test: The same procedure was followed as described above.

Acid calibration $y = 1.0666x - 0.3589$ where, y -axis= (A acid/ A I.S.) & x - axis= (C acid/ C I.S.)

Alcohol calibrations: $y = 1.1269x - 0.0878$ where, y -axis= (A OH/ A I.S.) & x - axis= (C OH/ C I.S.)

where, A acid = area of acid, A IS = area of internal standard, C acid = concentration of acid, C IS = concentration of internal standard, C OH = concentration of octadecanol

Table 10 GC-MS raw data along with calculations

Tests	acid	Alcohol (OH)	I.S.	C acid/ C I.S.	C OH/ C I.S.	Conc. acid	Conc. OH	# moles acid	# moles OH	Mass balance (%)
Acid mix with ceria	71151203	0	23293000	3.200372582	0	0.512059613	0	0.0001067	0	106.7
Alcohol mix with ceria	0	89763049	28554405	0	2.867495	0	0.458799	0	9.56E-05	95.6

GC-MS results of stearic acid hydrogenation

After the reaction was done, the reactor was left to cool to room temperature. Then the solids were separated by centrifugation and 1 ml of aliquot was derivatized with 0.25 ml sylon BFT at 70 ^{o}C for 1 h. Finally 60 µL of derivatized aliquot were mixed with 920 µL of hexane and 1-methylnonadecanoate (20 µL, 8 mM) as internal standard (I.S.) in gc vial and analyzed by GC-MS. Some reactions had solids (substrate and/or products) stuck on the reactor cover. After separating catalyst by centrifugation, the reactor was washed with known amount of hexane and analyzed by GC-MS. Washings were performed 2 times labeled as: wash I (4 ml hexane) and wash II (4 ml hexane). 4 ml of the washed samples were derivatized with 0.25 ml of Sylon BFT at 70 ^{o}C at 1 h and samples for GC analysis were prepared in the same manner as explained above.

Table 11 GC-MS results of hydrogenation activity by bare ceria

Conditions	acid	Alcohol (OH)	Aldehyde (CHO)	Alkanes (Alk.)	I.S.	# moles acid	# moles OH	# moles CHO	# moles Alk.	Total moles
250 °C,30 bar H_2, 0.5 h	3089432 7	3907626	1242209 1	584560	5450895 7	2.54995E-05	2.79482E-06	4.39132E-05	3.18814E-06	7.53956E-05
250 °C,30 bar H_2, 0.5 h wash I	2679795 3	2109389	4621260	0	5306594 4	8.08709E-06	6.83529E-07	3.04578E-06	0	3.17317E-05
250 °C,30 bar H_2, 0.5 h wash II	1312170	0	0	0	4962690 7	3.5733E-06	0	0	0	3.5733E-06
250 °C, 30 bar H_2, 1 h	3553755 3	2703622	1293020 6	824246	4488902 0	3.17386E-05	2.51337E-06	5.88E-05	4.4404E-06	9.75397E-05
250 °C, 30 bar H_2, 2 h	3653249 6	1008152	2601873 5	179581 5	6751491 5	2.47873E-05	1.40081E-06	8.3E-05	9.50167E-06	0.000118699
250 °C, 30 bar H_2, 3 h	4478589 1	4207850	2818008 0	124666 1	6659001 8	2.84342E-05	2.58611E-06	9.24E-05	6.64092E-06	0.000130057
230 °C, 30 bar H_2, 2 h	1151610 4	0	560059	242890	1151610 4	4.24768E-05	2.59761E-06	1.03482E-06	1.4119E-06	4.7504E-05
230 °C, 30 bar H_2, 2 h wash I	1502816 9	0	4328 41	0	1531130 3	4.18988E-05	2.59761E-06	0	1.46592E-07	4.24768E-05

Table 12 GC-MS results of hydrogenation activity by CuO/CeO_2 catalysts

Conditions	acid	Alcohol (OH)	Aldehyde (CHO)	Alkanes (Alk.)	I.S.	Mass balance (%)
0.23 Cu/Ce, 250 oC,5 bar, 2 h	801568	76869920	0	35585397	60244555	95.56
0.12 Cu/Ce, 250 oC,5 bar, 2 h	0	45213219	0	17299549	24592238	146
0.056 Cu/Ce, 250 oC, 5 bar, 2 h	0	168012358	0	1996507	66600218	98.81 (includes wash I)
0.056 Cu/Ce, 250 oC, 5 bar, 2 h wash I	780568	3456548	0	330173	12819843	
0.056 Cu/Ce, 235 oC, 5 bar, 2 h	79059974	5856169	0	1583865	87077060	70 (includes wash I)
0.056 Cu/Ce, 235 oC, 5 bar, 2 h wash I	55535476	3184791	0	407014	81355323	

CALIBRATION CURVES:

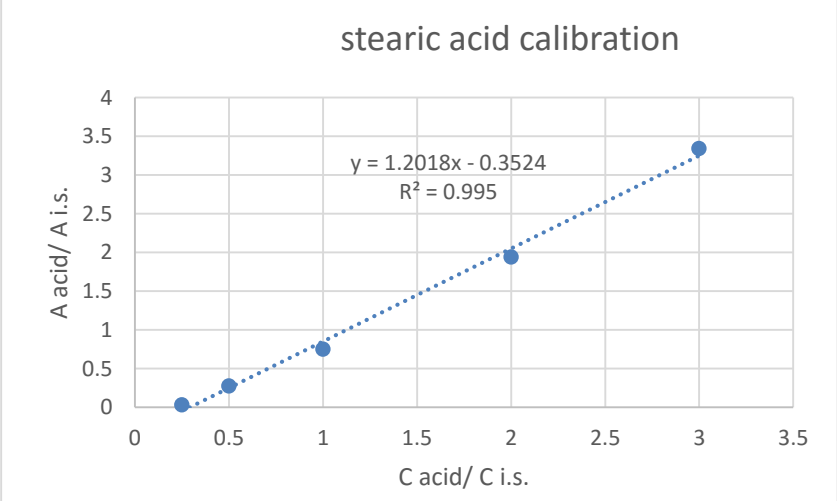

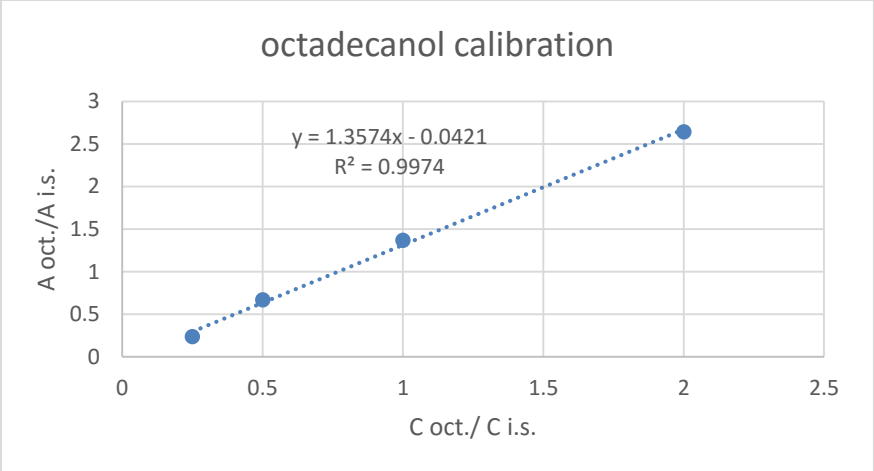
octadecanol calibration
y = 1.3574x - 0.0421
R² = 0.9974
A oct./A i.s.
C oct./ C i.s.
0
0.5
1
1.5
2
2.5
3

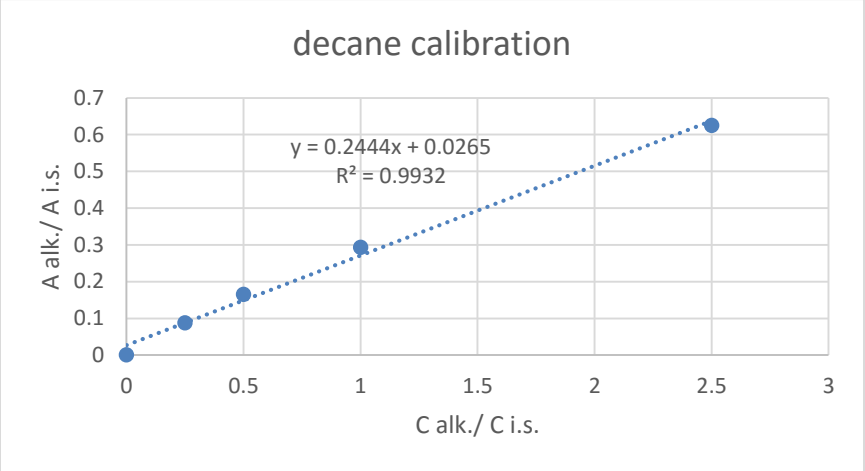
decane calibration
y = 0.2444x + 0.0265
R² = 0.9932
A alk./ A i.s.
C alk./ C i.s.
0
0.1
0.2
0.3
0.4
0.5
0.6
0.7
0.5
1
1.5
2
2.5
3

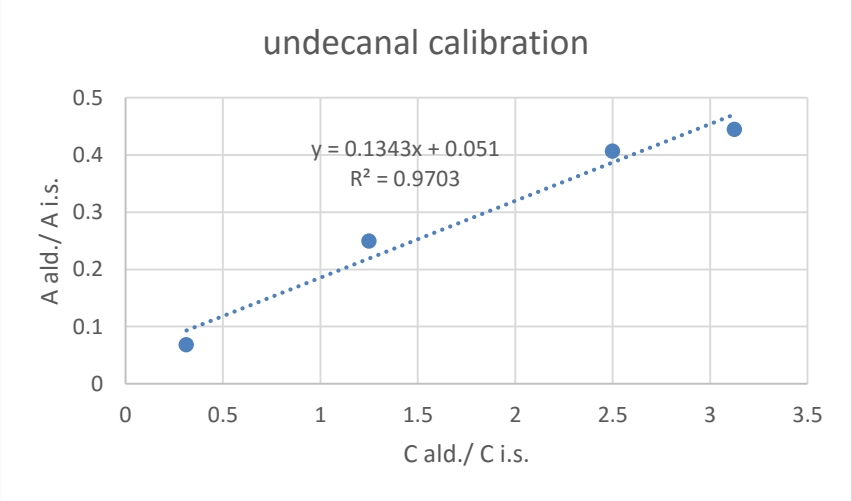
undecanal calibration
y = 0.1343x + 0.051
R² = 0.9703
A ald./ A i.s.
C ald./ C i.s.
0
0.1
0.2
0.3
0.4
0.5
0.5
1
1.5
2
2.5
3
3.5

APPENDIX B
DETERMINATION OF BASIC AND ACIDIC SITES BY TITRATION

Determination of basic sites by titration

Stock solutions: 0.01 M HCl, 0.0105 M NaOH
C-500 = 23.1 mg
C-700 = 24.4 mg
C-900 = 21.4 mg
The carbons were treated with 10 ml of 0.01 M HCl for over 24 h; separated by centrifugation and 5 ml of supernatant was back-titrated with 0.0105 M NaOH. A blank experiment was run by titrating 0.01 M (5 ml) HCl with 0.0105 NaOH. We used universal indicator in each titration to determine the end point.

Table 13 Titration results for basic sites determination

Samples	Initial volume (ml) A	Final volume (ml) B	Change in volume (ml) C= B-A	Net change in volume (ml) D = C-4.4
Blank	1.9	6.3	4.4	
C-500	6.3	10.25	3.95	0.45
C-700	10.25	13.7	3.45	0.95
C-900	13.7	17.45	3.75	0.65

Calculations

For C-500:

$$0.45\ ml * \frac{1\ L}{1000\ ml} * \left(\frac{0.0105\ mol\ NaOH}{1\ L}\right) * \frac{1\ mol\ HCl}{1\ mol\ NaOH} = 4.725\ micromoles\ in\ 5ml\ supernatant$$

In 10 ml: 2 * 4.725 micromoles in 23.1 mg C-500 => 0.4091 mmol/g basic sites in C-500
Similarly,
C-700 has 0.8176 mmol/g basic sites
And,
C-900 has 0.630 mmol/g basic sites

Determination of acidic sites by titration

Stock solutions: 0.01 M HCl, 0.01 M NaOH
C-500 = 24.3 mg
C-700 = 20.9 mg
C-900 = 23.2 mg
The carbons were treated with 10 ml of 0.01 M NaOH for over 24 h; separated by centrifugation and 5 ml of supernatant was back-titrated with 0.01 M HCl. A blank experiment was run by titrating 0.01 M (5 ml) NaOH with 0.01 M HCl. We used universal indicator in each titrations to determine the end point.

Table 14 Titration results for acidic sites determination

Samples	Initial volume (ml) A	Final volume (ml) B	Change in volume (ml) C= B-A	Net change in volume (ml) D = C-4.4
Blank	2.3	7.7	5.4	
C-500	7.9	12.6	4.7	0.70
C-700	12.6	17.6	5.0	0.40
C-900	17.7	22.7	5.0	0.40

Calculations

For C-500:

$$0.70\ ml * \frac{1\ L}{1000\ ml} * \left(\frac{0.01\ mol\ HCl}{1\ L}\right) * \frac{1\ mol\ NaOH}{1\ mol\ HCl} = 7.0\ micromoles\ in\ 5ml\ supernatant$$

In 10 ml: 2 * 7.0 micromoles in 24.3 mg C-500 => 0.576 mmol/g acidic sites in C-500
Similarly,
C-700 has 0.383 mmol/g acidic sites
And,
C-900 has 0.345 mmol/g acidic sites

Table 15 ICP result of iron supported on C-500

Material	Wt %
C-500	1.68